EUROPEAN LABORATORY FOR PARTICLE PHYSICS

CERN-PPE/97-100
28.7.97

THE CHORUS SCINTILLATING FIBER TRACKER AND OPTO-ELECTRONIC READOUT SYSTEM

P. Annis[a], S. Aoki[b], G. Brooijmans[c,1], J. Brunner[d], J. Dupraz[d], J. Dupont[d], J.-P. Fabre[d], D. Favart[c], W. Flegel[d], D. Frekers[e], G. Grégoire[c], M. Gruwé[a,2,3], J. Herin[c,1], K. Hoepfner[f,4], M. Kobayashi[g], J. Konijn[h], T. Kozaki[g], P. Lamonte[a] V. Lemaitre[c,4], P. Lendermann[f], D. Macina[d,5], R. Meijer Drees[d,6], L. Michel[c,1], C. Mommaert[a,1,3], K. Nakamura[i], M. Nakamura[g], T. Nakano[g], P. Nappey[d], K. Niwa[g], E. Niu[d,7], J. Panman[d], R. Pintus[d], F. Riccardi[d], S. Reynaud[d], D. Rondeshagen[e], O. Sato[g], G. Stefanini[d], G. Van Beek[a,1], M. Vander Donckt[a,8], P. Vilain[a,2], C. Weinheimer[d,9], G. Wilquet[a,2], K. Winter[f], H.T. Wong[d,0].

[a] Inter-University Institute for High Energies (ULB-VUB), Brussels, Belgium
[b] Kobe University, Kobe, Japan
[c] Université Catholique de Louvain, Louvain-la-Neuve, Belgium
[d] CERN, Geneva, Switzerland
[e] Westfälische Wilhelms-Universität, Münster, Germany
[f] Humboldt-Universität, Berlin, Germany
[g] Nagoya University, Nagoya, Japan
[h] NIKHEF, Amsterdam, The Netherlands
[i] Osaka City University, Osaka, Japan
[1] Inter-University Institute for Nuclear Sciences, Belgium
[2] National Foundation for Scientific Research, Belgium
[3] Now at CERN, Geneva, Switzerland
[4] Now at DESY, Hamburg, Germany
[5] Now at Université de Genève, Genève, Switzerland
[6] Now at University of Washington, Seattle, USA
[7] In part, Postdoctral Fellow for Research Abroad from Japan Society for the Promotion of Science, Japan
[8] Fonds de Recherche pour l'Industrie et l'Agriculture, Belgium
[9] Now at Johannes Gutenberg-Universität, Mainz, Germany
[0] Also at Institute of Physics, Academia Sinica, Taiwan

To be submitted to Nuclear Instruments and Methods

ABSTRACT

A scintillating fiber tracker system consisting of more than one million fibers has been successfully constructed and made operational for the CERN WA95/CHORUS experiment. The design and construction of the tracker system as well as its opto-electronic readout are described. The performance of the detector with high energy muons is presented.

1. Introduction

Neutrino masses and mixings, if they exist, will have profound implications in particle physics, astrophysics and cosmology [1]. The investigations of these fundamental neutrino properties remain one of the great challenges in experimental particle physics. The objective of the CERN WA95/CHORUS experiment [2] is to search for neutrino oscillations in the $\nu_\mu \rightarrow \nu_\tau$ appearance channel with the CERN SPS wide band neutrino beam.

The CHORUS experiment was approved in September 1991. The construction of the detector was completed by November 1993 when a technical run with a dummy target was conducted. Physics data taking with complete emulsion target started in May 1994, and will last until the end of 1997. A detector efficiency (detector operational when beam is delivered) of 83.5% has been achieved in the 1994-95 runs, and was further improved to 94% in 1996. The inefficiency due to data acquisition dead time is not included.

The schematic diagram of the CHORUS detector [3] is depicted in Figure 1. A total of 800 kg of nuclear emulsion is used as target material. The signature for $\nu_\mu \rightarrow \nu_\tau$ oscillation is the explicit vertex detection of the charged current interaction $\nu_\tau N \rightarrow \tau^- X$ and the subsequent decay kink of the short-lived τ^- to its daughters, shown schematically in Figure 2. With 4 years of data taking, the experiment is expected to achieve a sensitivity of $\sin^2 2\theta_{\mu\tau} \sim 2 \times 10^{-4}$ at large $\Delta m^2_{\mu\tau}$, an interesting parameter space for the hypothesis of ν_τ as a Dark Matter candidate [4]. The $\Delta m^2_{\mu\tau}$ versus $\sin^2 2\theta_{\mu\tau}$ parameter space to be explored by CHORUS, together with regions excluded by previous experiments [5], is shown in Figure 3.

The experimental set-up consists of the emulsion target, a scintillating fiber tracker system, an air-core magnet [6], a lead/scintillating fibers calorimeter [7], and a muon spectrometer. The emulsion target, tracker system and magnet are placed in a "cold box" with temperature stabilized at 5°C, in order to reduce fading of the emulsion as well as the possible ageing of the scintillating fibers.

Nuclear emulsions offer a superb spatial resolution of 1 μm with a hit density of 300 mm^{-1}, and is therefore ideal for the detection of short-lived particles. The fiber tracker system provides accurate trajectory predictions back to the emulsion target, as well the two-track resolution necessary for event reconstruction. Together with the magnet, the tracker also allows measurement of charge and momentum of the traversing particles. Coupled to the kinematical information provided by the calorimeter and spectrometer, events with kinematics resembling the ν_τ charged-current interactions can be pre-selected for emulsion scanning to reduce the required scanning time. The kinematics

measurements also provide further constraints to identify and reject the various background events with kinks topology such as those due to charm decays.

2. The CHORUS Fiber Tracker System

2.1 Scintillating Fiber Tracker

The first large scale scintillating fiber tracking detector was built for the UA2-upgrade [8], consisting of 60000 fibers of 1 mm in diameter. The CHORUS tracker system [9] expands its application by more than an order of magnitude. It is based on a total of about 1.2 million plastic scintillating fibers of 500 μm diameter and 2.3 m length (comprising 1.6 m of useful detector element and 0.7 m of flexible light guide). The fibers [10] consist of a polystyrene core (refractive index 1.59) doped with 1% butyl-PBD [1] and 0.1% BDB [2], surrounded by a 3 μm PMMA [3] cladding (refractive index 1.42) to provide internal reflection. The emission spectrum peaks at about 420 nm. Fiber ribbons with 7 layers in the "staggered" geometry as shown in Figure 4, are constructed using a specially designed fiber-winding machine [11]. Each layer is painted with a TiO_2-based white paint, which acts both as a glue and as an extra-mural absorber (EMA) to prevent cross-talk. The far ends of the ribbons are polished and sputtered with aluminum. The reflectivity thus obtained is about 80%. The procedures and quality control of the mass production of the fiber-ribbon have been reported elsewhere [12].

The scintillating fiber technology was selected for the CHORUS tracker because of its good spatial resolution and two-track resolution, while its relatively modest cost (at about 2.5 CHF per fiber-channel including readout and electronics) provides another attractive feature. Fibers of 500 μm diameter were chosen after optimization between light yield, attenuation length and spatial resolution. The basic structure of 7 fibers per ribbon ensures excellent response for traversing minimum ionizing particles.

The principal design objectives of the CHORUS tracker system are : a) to produce predictions for a subset of tracks from the neutrino interaction vertices at the interface emulsion sheets with the highest angular and position accuracies for further location of the

[1] butyl-2-phenyl-5(4-biphenylyl)-1-3-5-oxadiazole

[2] 4,4'-bis-(2,5-dimethylstyryl)-diphenyl

[3] polymethyl methacrylate

events in the emulsion target (rather than to disentangle all tracks including secondaries and showers); and b) to provide measurements of the charge and momentum of hadrons, and in particular those from the decays of the τ^- leptons created in the ν_τ charged-current interactions.

The tracker system consists of two components:

1. **The target tracker**
   There are four emulsion target stacks and eight target tracker ("TT") modules, half of which is shown schematically in Figure 5. Each tracker module consists of four projection planes (Y, Z, and $Y^{\pm}$, $Z^{\pm}$ rotated by $\pm 8^\circ$ relative to Y, Z), and each projection is constructed using the 7-layer ribbons. The geometry of a "non-inclined" and an "inclined" projection is displayed in Figure 6. There are 8 target tracker modules altogether, interleaved between the 4 target emulsion stacks, as depicted in Figure 5. Coupling the information from the four projections together, a three-dimensional trajectory can be uniquely measured for each traversing particle.
   The major role of the target tracker is to reconstruct the position of the neutrino interaction vertices, and to make accurate predictions for tracks locations and directions at the interface emulsion sheets (shown as CS in Figure 2), both of which are essential for track scanning and following in the emulsion target. The separation between the target emulsion and the closest downstream tracker modules (40 mm) is an optimization from two conflicting requirements : the two-track separation of the tracker and the accuracy of the track prediction. The good two-track resolution of the fiber trackers allows a relatively compact design with good geometrical acceptance, as compared to other tracking detectors such as drift chambers (see 3.3).

2. **The "diamond-shaped" magnet tracker**
   As displayed in Figure 7, there are three magnet tracker ("DT") modules, one upstream and two downstream the hexagonal toroidal air-core magnet [6], which has a field of 0.12 T, an axial length of 0.75 m and an external radius of 1.5 m (such that the sagitta for a 1 GeV particle is 2.5 mm). Each tracker module is hexagonal and consists of two planes. Three adjacent "paddles" arranged in the geometry shown in Figure 8 constitute one plane; each paddle measures one of three coordinates at 120° from each other. The second plane measures the complementary coordinates at 60° from the first. Paddles are made up of the 7-layer ribbons. Both the magnet and the tracker have the same six-fold symmetry such that one of the two coordi-

nates measured by each module is in the bending plane. Based on the curvature of traversing particles through the magnet, the magnet tracker measures the charge and momentum of particles (in particular, of the daughters from the decay of the τ) which originate from a neutrino interaction in the target. This information, together with measurements from the calorimeter and spectrometer, is essential in reducing the size of the sample of $\nu_\tau N$ candidate events to be scanned in the emulsion and in differentiating them from the background events with kink topology, such as those due to charm decays and to pion elastic scattering without visible recoil ("white kink").

2.2 Opto-electronic Readout System

The choice of opto-electronic as the readout device for the 1.2 million channels of fibers allows a cost-effective system to be built. The key ingredient is the capability to measure individual photo-electrons with spatial information from the scintillating fibers. The relatively slow readout speed is not critical to the CHORUS application due to the low rate of neutrino events (about 0.5 neutrino events in the target region per neutrino spill with a typical width of 4 ms).

As shown in Figure 9, the readout ends of 16 fiber ribbons are bundled together and coupled to the opto-electronic readout chains, comprising four image intensifiers and a CCD camera [13] in series, as depicted schematically in Figure 10. A total of 58 such chains are needed to readout the entire fiber tracker system. To minimize the perturbations due to external magnetic fields, the chain is assembled inside a shielding made of mu-metal and soft iron. This shielding reduces the ambient magnetic field at the position of the first photocathode by a factor of 5 to 10, depending on the orientation of the external fields with respect to the optical axis of the chain. Detailed descriptions of the properties of the image intensifiers [14], as well as the CCD cameras and their data acquisition [15] are documented in the references listed.

The characteristics of the four image intensifier stages are summarized in Table 1. The detection efficiency of a photon emitted by the fibers is determined by the quantum efficiency (QE) of the first stage (an electrostatic demagnifier from 100 mm to 25 mm), and is measured to be about 18%, which is a convolution of a photo-cathode QE of 22% and a phosphor QE of 80%. A medium-slow phosphor P11 (50/90% light collection in 50/500 μs) is chosen for the first stage so that only a negliglible amount of light is lost

in the first 0.5 μs due to trigger delay. The phosphor for all other stages is the fast P46 (complete light collection in 1 μs). The photo-cathode of each stage is optimized to match the spectral emission of the phosphor of the preceeding stage. Background considerations restrict integration time of the gaetable Micro-Channel Plate (MCP) to be 20 μs or less, corresponding to the collection of about one-third of the light emitted by the first stage. Accordingly, the second electrostatic stage is inserted to boost the gain before the MCP to avoid loss of signal with this gate time. The final demagnifying stage brings the images onto the CCD sensor and camera, giving an overall demagnification factor of 0.11. Considering the intrinsic gain for each stage and the coupling loss between them, the net gain for the entire assembly of image intensifiers is about 10^4 to 10^5.

Image intensifier	II_1	II_2	II_3	II_4
Type	Electrostatically focused	Electrostatically focused	MCP proximity focused (gateable)	Electrostatically focused
Cathode Diameter	100 mm	25 mm	25 mm	25 mm
Magnification	0.20 to 0.25 (adjustable)	1	1	0.44
Screen Phosphor Emission Peak	P11 460 nm	P46 530 nm	P46 530 nm	P46 530 nm
Quantum Efficiency (photocathode + input window)	22.3 % at 430 nm	17.2 % at 460 nm	11.0 % at 520 nm	12.8 % at 530 nm
Gain	126 γ/γ at 430 nm	7.5 γ/γ at 460 nm	$\sim$ 800 γ/γ at 520 nm at V_{screen} = 6 kV and V_{MCP} = 750 V	8.7 γ/γ at 530 nm
Limiting resolution at input	13 lp/mm	70 lp/mm	35 lp/mm	31.5 lp/mm

Table 1 Characteristics of the CHORUS image intensifiers.

The sensor contains an image zone and a memory zone, with an antiblooming facility in the image zone to provide fast clear capabilities in 1 μs. Each zone consists of

550×288 pixels with dimension 16×23 μm^2, corresponding to 145 μm $\times$ 209 μm in detector space. Pixels are oriented with their narrow side across the beam direction. The transfer time from the image zone to memory zone is about 125 μs, while the readout of one image, done during the intervals between neutrino spills (either 2.5 s or 12 s), takes about 20 ms. Therefore, the system can record two events in a neutrino spill which has a typical width of 4 ms.

Number of pixels	550 rows $\times$ 288 lines = 158400 pixels
Pixel total dimension	16 μm(H) $\times$ 23 μm(V)
Pixel active dimension	12 μm(H) $\times$ 23 μm(V)
Spectral response :	
Response peak	800 nm
Quantum efficieny at 530 nm	$\sim$ 15%
Noise level (20 ms integration time at 20°C) :	
	102 photoelectrons / pixel
Linearity	linear up to 40% of full illumination (100%)
Timing :	
Fast clearing	1 μs
Transfer image to memory zone	125 us
Readout time	20 ms
Image processing and compression	$\sim$ 1 s
Event size (for entire 58 chains) :	
Neutrino event	150 kbyte
Cosmic calibration event	150 kbyte
Fiducial calibration event	450 kbyte

Table 2 Characteristics of the CHORUS CCD sensor and camera.

The schematic diagram of the CCD readout and data acquisition system [15] is depicted in Figure 11. The performance characteristics are given in Table 2. The video output of the CCD sensor is digitized with an 8-bit ADC at a Video Signal Processing (VSP) board mounted near the image intensifiers and CCD sensor assembly. The 58 CCD cameras are driven by trigger electronics and two clock generators (labelled "ODD" and "EVEN" in Figure 11) located at the experiment control room. The digitized CCD

data and the synchronization signals are transported over 26 m long cables between the detector and the control room. The 8-bit digitized signal from two cameras are combined into a 16-bit wide data by a specially designed "Translator" module. This module combines the data with their corresponding synchronization signals according to a Video Bus (VIB) protocol and transfers them to the commercial VME-based SL30 [16] slave processor modules. A total of 29 SL30 modules are required to read out the 58 image intensifier and CCD chains. Images of individual chains can be displayed on a color monitor, via a VME-based Image Processing Port (IPP [16]). The SL30 modules perform on-line data processing and compression during the time between neutrino spills and this typically requires 1 s per event. The compressed data is assembled by a local CPU (FIC8234 [16]) and then transferred to the central CHORUS data acquisition system. Various online histograms (displaying information such as the noise levels, pulse height and efficiencies of all the readout chains) are used to monitor the performance and stability of the system.

The data acquisition dead time is due to the 125 μs transfer time after the first event, and the event number limit of two in a neutrino spill. With a typical event rate of 0.5 per spill, the dead time due to the opto-electronic readout is about 6% (with approximately equal contributions from the transfer time and from the event number limit).

2.3 Calibration System

The image distortion of the opto-electronic readout system discussed above is sensitive to residual magnetic field which is not completely shielded, as well as to electrostatic build-up among the electrodes inside the image intensifiers (it may take several hours of operation before the field configuration reaches an equilibrium state). A calibration system is therefore necessary to obtain an accurate mapping between the input window and the CCD pixel coordinates, and to compensate for its time variation.

A total of 16 fiber ribbons are bundled together at the readout end, with spacers separating adjacent ribbons, as depicted in Figure 9. The spacers have a thickness of 200 μm, except five which are 500 μm in thickness, and contain 45 clear fibers (9 per spacer) of 127 μm in diameter. These "fiducial" fibers are grouped together and coupled through a fiber optic cable to a LED pulser module. Details of the construction and tests of the calibration system can be found in reference [17].

The exact dimension of the fiber bundles and the positions of the fiducial fibers were measured with photographic contact prints before the opto-electronic readout chains were

mounted on to the fiber bundles. Their geometry is shown in Figure 12 which also shows how the input pattern is distorded by the electrostatic field of the image intensifiers chain. By measuring the positions of the fiducial fibers and comparing them with their contact print coordinates, a fit for the distortion correction can be performed using the expression $R_{CCD} = AR_{in}(1 + B(R_{in}/R_0)^{\alpha})$, where R_{CCD} and R_{in} represent the radial positions of the fiducial fibers on the CCD and on the input window from the optical centers, respectively, and $R_0 = 5$ cm is the radius of the input window. The fitted parameter $A(\sim 0.1)$ describes the demagnification of the opto-electronic readout chain, whereas $B(\sim 0.25)$ and $\alpha(\sim 2.7)$ parametrize the distortion. The residuals of the fit have a $\sigma \sim 110\,\mu$m at the input window.

The fiducial fiber system is also used for optimization of the operation parameters for the opto-electronic readout. The LED intensity is adjusted to produce single photoelectrons at the first photocathode of the readout chain. The optimal operation parameters, such as the image intensifier focus and zooming voltages as well as the MCP voltage and gate time, can be determined by studying the response (such as the quantum efficiencies, gain, spatial resolution, and signal-to-noise ratio) of the readout system. During normal operation, calibration data with the fiducial fiber system are taken typically once every few minutes, and the various quantities which characterize the performance and stability of the opto-electronic readout system are continuously monitored.

2.4 Detector Alignment

Muons with an average energy of about 25 GeV are produced by the neutrino interactions upstream of the detector. These muons pass through the detector and can be used for measuring the properties of the fiber trackers, as well as for achieving precise relative alignment of the various tracker planes.

To achieve the required precision, the geometry of the fiber trackers must be accurately known. Fiber positions within a ribbon are measured during construction [11]. The deviation from straightness of each ribbon (the so-called "banana" effect) is measured and parametrized by a polynomial to be used in subsequent correction factors. The relative alignment between various ribbons in the same or different target tracker planes is based on the beam muon data [18]. This is achieved by minimizing, with the MINUIT software package [19], the square of the hit residual sum over a large sample of events, allowing for relative translation and rotation of different tracker planes as well as relative trans-

verse translation among different ribbons in the same plane. The longitudinal positioning among the various planes is performed similarly, but is based on the cosmic ray data which provide tracks crossing the detector at large angle. This alignment procedure is carried out typically once every two months during data taking, so that variations with time can be monitored.

Inter-calibration between the target trackers and the interface emulsion sheets is performed during the startup phase of the experiment. Two complementary methods are employed. The first one is the measurement with the trackers of a set of reference positions known to a precision of 60 μm and produced by beta-ray guns inserted in the honeycomb boards supporting the sheets emulsion. These references are then compared with emulsion marks generated by X-ray guns located at the same positions. In addition, several hundreds of beam muons are located at the interface sheets and compared with predictions from the target trackers. The combined data set are used to evaluate the relative scaling, translation and rotation coefficients between the target tracker system and the interface emulsion sheets.

For the magnet tracker modules, the position of each individual fiber in one paddle (16 ribbons) is known with a precision of 50 μm, by construction and microscope measurement of two reference fibers per ribbon. The positions of the six paddles in a tracker module and of the tracker in the detector frame has been obtained by standard optical survey techniques with a precision of about 0.5 mm. The final alignment of the magnet tracker modules with respect to the target tracker has been made with beam and cosmic muons as explained above, allowing for rotation, tilt and translation of each paddle independently.

3. Detector Performance

3.1 Intrinsic Characteristics of Fibers and Readout

The performance of the opto-electronic readout can be measured based on data from the fiducial calibration system independent of the fiber trackers. By comparing with the measurements using a photo-multiplier with known quantum efficiency, the quantum efficiency (ratio of the detected photo-electrons at the CCD level to the amount of incoming photons at the first image intensifier stage of the opto-electronic chain) is determined to be about 18%. There are two aspects which characterize the spatial resolution of the

readout system. The "spot size", (the width of the charge distribution induced on the CCD from a single photo-electron in the first image intensifier) is due to the intrinsic resolution of the image intensifier stages plus the finite CCD pixel size, whereas the "spot displacement" (the deviation of the measured center of gravity of a hit-cluster from its mean position) is caused mainly by the imperfection of the focusing of the individual photo-electrons in the first image intensifier. Based on measurements with the fiducial fibers, the standard deviations for the spot size and displacement are 136 μm and 89 μm at the input window, respectively.

The muons associated with the neutrino beam provide clean minimum ionising particles for the measurement of the intrinsic properties of the scintillating fibers. The signatures of a "track-element" recorded by the CCD when such beam muons traverse a 3 mm fiber thick ribbon are depicted in Figure 13. The crosses superimposed on the display are the "hits" as identified by software "clustering" algorithms [20], corresponding to detected single photo-electrons.

The ribbon hit density (Y) as a function of distance (x) from the readout is shown in Figure 14. The distribution can be described by

$$\mathrm{Y} = \frac{\mathrm{A}}{1+\mathrm{r}}\,[\,\exp(-\frac{(\mathrm{x}-\mathrm{L})}{\lambda}) \;+\; \mathrm{r}\times\exp(-\frac{(\mathrm{L}-\mathrm{x})}{\lambda})\,]\;.$$

where L=230 cm is the length of the fiber, and r=0.8 is the mirror reflectivity at the far end of the fiber. The fitted quantity A denotes the hit density at x=L ($\sim$ 5 hits per ribbon), whereas $\lambda \sim 220$ cm is the "bare" attenuation length of the scintillating fibers. The "effective" attenuation length can be evaluated by fitting the distribution to a single exponential, and is measured to be $\lambda_{eff} \sim 600$ cm. From Figure 14, it can be seen that the hit density is about 5 and 7 hits/ribbon at the far (230 cm) and near (70 cm) ends of the detector, respectively.

The tracker detector inefficiency per ribbon (the probability of a minimum ionizing particle passing through without producing any signals recorded by the CCD) is measured using the beam muon data, to be about 2×10^{-3}. This is consistent with the expectation from Poisson statistics based on a measured mean of 5 to 7 hits per ribbon.

There is cross-talk (or "signal associated noise") in the system, attributed to the fact that the entrance fiber optics window to the first image intensifier stage (the 100/25 demagnifier) is not equipped with extra-mural absorber (EMA) due to unavailability at the time of manufacture. Spurious but isolated hits may show up as distant as 1 mm from the actual track-elements. The distribution of the distance between the individual hits left by a charged particle and the best fitted trajectory from raw data is gaussian

like with large tails as seen in Figure 15. About 20% of the hits are found at a distance greater than 600 μm, where the standard deviation of the gaussian is $\sim$360 μm. Most cross-talk hits can be distinguished and rejected before subsequent analysis by imposing a maximum distance cut from the track-elements or a minimum length cut within the ribbon since they always manifests themselves as single isolated hits.

By monitoring the measured attenuation length of the fibers as a function of time, the ageing effects can be deduced. As shown in Figure 16, the attenuation length as well as the hits ratio between the "far" and "near" ends of the ribbons have been monitored and no deterioration have been observed over a course of 30 months . This satisfactory result can be attributed to the special attention paid during the construction and operation of the tracker system - minimizing exposure to ultra-violet light, handling with clean gloves, as well as storage and operation in a 5°C ambient temperature.

3.2 Stability in Operation

The precision of the system is sensitive to the mapping between the CCD pixel coordinates with their corresponding locations at the input window, which is based on measurements of the fiducial fibers and the distortion correction procedures as described in Section 2.3.

In the course of operation, it was discovered that there are occasions where this mapping is not stable with time, thus making it necessary to evaluate the mapping parameters once per run, which lasts typically 90 minutes. Two observations are particularly noteable:

1. When an opto-electronic chain is switched on after long (more than several hours) shut-down, it may take as long as one day for its internal electrostatics to reach a steady state. The translational shifts during this period can be as big as 2 mm at the input window. Not all chains show this behaviour, and for those which do, the effect may not be identical at the different trials of switching on so that the eventual equilibrium positions may be different. This effect can be calibrated with a run-by-run distortion correction measurement.

2. In the 1994-95 data taking, the air-core magnet gave a stray field at the opto-electronic location ($\sim$ 2 G for the DT chains) due to an unexpected asymmetry in the current flow of the magnet. This stray field gave rise to a transient rotation of the fiducial pattern during and after the pulsing of the magnet, as depicted in

Figure 17. Fiducial fiber measurements had to be made at the magnet pulsing to provide correction factors for this effect, which can be as large as 500 μm at the opto-electronic input window of the magnet trackers. In the 1996-97 data taking, a compensation coil was added to the magnet to suppress the stray field, and the measured rotational angle of the fiducial fibers image was reduced by a factor of 5, also shown in Figure 17.

The other parameters characterizing the performance of the system, like the fiber light yield and attenuation length displayed in Figure 16, as well as the gain, quantum efficiencies, spot size and displacement of the opto-electronic readout, are found to be stable in the course of the experiment. The component which requires regular attention is the micro-channel plate (MCP). This device has a finite life time depending on its previous history (for instance, a prolonged intense light input may shorten its life). Typically, one to two MCPs (out of a total of 58) have to be replaced in six months of operation.

3.3 Performance with Muon Beam

Data of muons associated with the neutrino beam are taken at a regular interval of typically once a month. The clean signatures provide the appropriate tools for the purpose of monitoring and alignment. The performance of the fiber tracker system in a muon beam thus indicates the intrinsic capability of the device for energetic, minimum ionising particles.

After the alignment procedures as described in Section 2.4 and with the hits due to cross-talk removed, the achieved hit residuals for beam muons (deviation of hits from the best fitted trajectory) has a $\sigma \sim 330\,\mu$m, while the "track-element" (the center of gravity of all hits in one ribbon) residual has a $\sigma \sim 185\,\mu$m, as shown in Figure 18.

The two-track resolution is not directly measurable with the beam muons. However, one can infer this value by adding the hit-residual and the spot-size contributions in quadrature, giving a combined $\sigma_{tt} \sim 380\,\mu$m. Adopting the criteria that two Gaussians can be distinguished when the "peak-to-valley" ratio of their sum is more than 2, two parallel tracks can be separated when they are 3.5 σ_{tt} or about 1 mm apart.

Beam muons have been located at the interface "changeable" sheets. The prediction accuracies (deviation of the target tracker predictions on the emulsion sheets from the found tracks) has a $\sigma \sim 150$ μm in position and ~ 2.5 mrad in angle, as depicted in

Figure 19. Folding in an expected intrinsic resolution of 1.5 mrad for the emulsion sheets, the angular resolution of the fiber tracker has a $\sigma \sim 2$ mrad.

A global fit is performed over the last three target tracker modules (12 projection planes) placed behind the last emulsion target and the three magnet trackers (6 projection planes) for high energy neutrino beam associated muons with the magnet turned off. Track-elements residuals for DT1,2,3 have standard deviations of 177 μm, 133 μm and 126 μm, respectively, as shown in Figure 20. It has been checked by Monte-Carlo simulation that these residuals can be explained by a common 180 μm intrinsic resolution and by the geometrical arrangement of the trackers and the sources of multiple scattering along the beam line.

The momentum resolution $\frac{\Delta p}{p}$ of the magnet tracker results from the quadratic combination of two terms : a constant term, evaluated at 22%, from the multiple scattering in the traversed material (mainly the front and back faces of the magnet) and a term proportional to the momentum which reflects the measurement accuracy. The value expected for this term from the intrinsic tracker resolution is $(\frac{\Delta p}{p})_{expect} = 2.5\% \times p$ Gev/c. Beam muon data are also taken with the air-core magnet being pulsed. By comparing with the momentum measured by the muon spectrometer system, the resolution of the magnet trackers can be evaluated. Displayed in Figure 21 are the RMS values of the relative difference between the measurements by the muon spectrometer and by the magnet tracker as a function of the spectrometer momentum. This distribution is well reproduced by convoluting the known spectrometer resolution ($\frac{\Delta p}{p} \sim 7\%$ below 6 GeV/c, where the range of the stopping muon is used, and $\sim 16.5\%$ above 6 GeV/c, where the curvature is measured) with a momentum dependent term given by $(\frac{\Delta p}{p})_{meas} = 3.5\% \times p$ GeV/c and with the constant term of 22%, as indicated by the solid line in Figure 21. The dashed line shows the momentum resolution of the magnet tracker. The charge of particles with momentum of 5 GeV/c can then be determined with a confidence level better than 99.9% Residual alignment problems such as imperfect planarity and thermal effects caused by the magnet pulsing are currently being investigated as possible sources of this discrepancy from the expected resolution.

3.4 Event Reconstruction in the Neutrino Beam

Reconstruction of events from neutrino interactions at the emulsion target is substantially more complex than that for traversing muon events. A typical ν_μ charged current

interaction recorded in the CHORUS experiment is depicted in Figure 22, indicating the final state muon and the hadronic shower. The neutrino interactions give rise to events with high multiplicity where the outcoming trajectories can be close to each other, especially in the target tracker region. The signal-related spurious hits mentioned in Section 3.1 further increase the combinatorics which have to be dealt with. Before reaching the magnet trackers, the particles from the primary vertices have to go through as much as 4 stacks of emulsion (11.2 cm in thickness, corresponding to 4 radiation lengths and 0.3 interaction lengths), degrading their energies and suffering from multiple scattering along the way. In addition, electromagnetic and, with a smaller probability, hadronic showers may develop in the emulsion stacks, further complicating the tracking procedures downstream. The wide energy and angular ($\pm$500 mrad relative to the neutrino beam axis) ranges where track reconstruction has to apply also add complexity to the algorithms and worsen the performance relative to those achieved in the ideal situations of high energy muons as described in Section 3.3.

The performance of the tracking system for the reconstruction of neutrino events will be the subject of a forthcoming publication.

4. Conclusion

The CHORUS Tracker has been successfully constructed and commissioned on schedule. It is the largest tracking system based on scintillating fibers ever built. After the initial debugging phase, operation has been smooth and the required efforts for maintenance have been light. The expected hardware performance in terms of hit density, fiber attenuation length and readout spatial resolution have been achieved. Correction for the electrostatic distortion of the opto-electronic readout has been performed to the required accuracy. Tracking performance in terms of hit and track-element residuals based on data from the neutrino beam associated muons also reaches the designed goals.

The first physics results from the CHORUS experiment have been reported [21] , demonstrating that the experiment as a whole works according to expectation, and that the designed sensitivities will be within reach. The "hybrid" detector concept of combining together information provided by the nuclear emulsion and the scintillating fiber trackers has been demonstrated, leading to two other future projects (Fermilab experiments E803/COSMOS [22] and E872/DONUT [23]) which have adopted similar approaches

and techniques. The forthcoming long baseline neutrino oscillation experiment (KEK-E362/K2K) which sends the KEK neutrino beam to the Super-Kamiokande detector [24] also employs, as a component of its near detector, the scintillating fiber trackers and opto-electronics readout similar to the CHORUS system.

The authors would like to thank D. Bonekämper, D. Bourillot, G. Carnevale, M. de Jong, J. Domeniconi, D. Eckstein, R. Ferreira, B. Friend, J.-L. Garavel, C. Gentet, M. Litmaath, H. Meinhard, F. Peron, G. Roiron, C. Rosset, A. van Hove, C.A.F.J. van der Poel, H. von Heynitz, J. Visschers and T. Wolff from the participating institutes, for their invaluable support with the mechanics, trigger, electronics and computing aspects of the construction and operation of the detector.

We are also indebted to the SPS staff for the efficient accelerator operation, to L. Gatignon for the West Area test beams, and to C. Lasseur and the CERN survey group. The general technical support from the PS, SPS, ECP and CN Divisions is warmly acknowledged.

We gratefully acknowledge the financial support of the different funding agencies: in particular, the Institut Interuniversitaire des Sciences Nucleaires and the Interuniversitair Instituut voor Kernwetenschappen (Belgium), the German Bundesministerium für Bildung und Forschung under contract numbers 05 6BU11P for Berlin and 05 7MS12P for Münster (Germany), the Japan Private School Promotion Foundation and Japan Society for the Promotion of Science (Japan), the Foundation for Fundamental Research on Matter FOM and the National Scientific Research Organisation NWO (the Netherlands).

References

[1] For an overview on the subject of neutrino physics, see, for example, "Neutrino Physics", ed. K. Winter, Cambridge University Press (1991) ;
For the current status of neutrino physics, see, for example "Procs. of the XVII Int. Conf. on Neutrino Physics and Astrophysics, Helsinki 1996", ed. M. Roos, World Scientific (1996).

[2] N. Armenise et al., CHORUS Proposal, CERN-SPSC/90-42, (1990);
M. de Jong et al., CHORUS Collaboration, CERN-PPE/93-131 (1993).

[3] E. Eskut et al., CHORUS Collaboration, in preparation for Nucl. Instrum. Methods.

[4] Ya. B. Zel'dovich and I.D. Novikov, Relativistic Astrophysics, Nauka, Moscow, 1967;
H. Harari, Phys. Lett. **B216**, 413 (1989);
J. Ellis, J.L. Lopez, and D.V. Nanopoulos, Phys. Lett. **B292**, 189 (1992);
H. Fritzsch and D. Holtmannspötter, Phys. Lett. **B338**, 290 (1994).

[5] N. Ushida et al., Phys. Rev. Lett. 57, 2897 (1986);
M. Gruwé et al., Phys. Lett. **B 309**, 463 (1993);
K.S. McFarland et al., Phys. Rev. Lett. 75, 3993 (1995);
P.F. Loverre, Phys. Lett. **B 370**, 156 (1996).

[6] F. Bergsma et al., Nucl. Instrum. Methods **A 357**, 243 (1995).

[7] S. Buontempo et al, Nucl. Instr. and Meth. A 349, 70 (1994);
E. Di Capua et al, Nucl. Instr. and Meth. A 378, 221 (1996).

[8] R.E. Ansorage et al. Nucl. Instrum. Methods **A 265**, 33 (1988);
J. Alitti et al., Nucl. Instrum. Methods **A 279**, 364 (1989).

[9] S. Aoki et al., Nucl. Instrum. Methods **A 344**, 143 (1994);
P. Annis et al., Nucl. Instrum. Methods **A 367**, 367 (1995).

[10] Scintillating fibers SCSF-38, Kuraray, Japan.

[11] T. Nakano et al., in *Proc. of IEEE 1991 Nuclear Science Symp.*, Santa Fe (1991).

[12] T. Nakano et al., in *Proc. of Scintillating Fiber Symposium 1993*, University of Notre Dame (1993).

[13] Image intensifier and CCD suppliers:
(100/25) electrostatic - Hamamatsu Photonics, Japan;
(25/25) and (25/11) electrostatic - Delft Electronische Produkten (DEP), The Netherlands;
(25/25) MCP - Proxitronic Funk, GmbH & Co., Germany;
CCD sensor - Thomson TH7864, Thomson, France.

[14] M. Gruwé, Ph.D. Thesis, Université Libre de Bruxelles (1994).

[15] C. Mommaert, Ph.D. Thesis, Vrije Universiteit Brussel (1995).

[16] VME-based modules:
SL30 - Eltec, Mainz, Germany;
IPP - Eltec, Mainz, Germany;
FIC8234, Creative Electronic Systems, Geneva, Switzerland.

[17] D. Rondeshagen, Dipl. Thesis, Westfälische Wilhelms-Universität (1994).

[18] G. Brooijmans, CHORUS Internal Notes (1996).

[19] MINUIT : Function Minimization and Error Analysis, Application Software Group, CN Division, CERN.

[20] P. Lendermann, Ph.D. Thesis, Humboldt-Universität (1994).

[21] K. Niwa, CHORUS Collaboration, in "Procs. of the XVII Int. Conf. on Neutrino Physics and Astrophysics, Helsinki 1996", ed. M. Roos, World Scientific (1996) ;
C. Weinheimer, CHORUS Collaboration, in "Procs. of the Int. Conf. on High Energy Physics, Warsaw 1996", ed. A. Wróblewski, World Scientific (1996), also as CERN-PPE/96-196 .

[22] K. Kodama et al., Fermilab Proposal P803 (1993);
K. Kodama et al., Update Report on Fermilab E803 (1995).

[23] B. Lundberg et al., Fermilab Proposal P872 (1994).

[24] Y. Fukuda et. al., Proposal for a Long Baseline Neutrino Oscillation Experiment using KEK-PS and Super-Kamiokande, KEK-E362 Proposal, 1995.

List of Figures

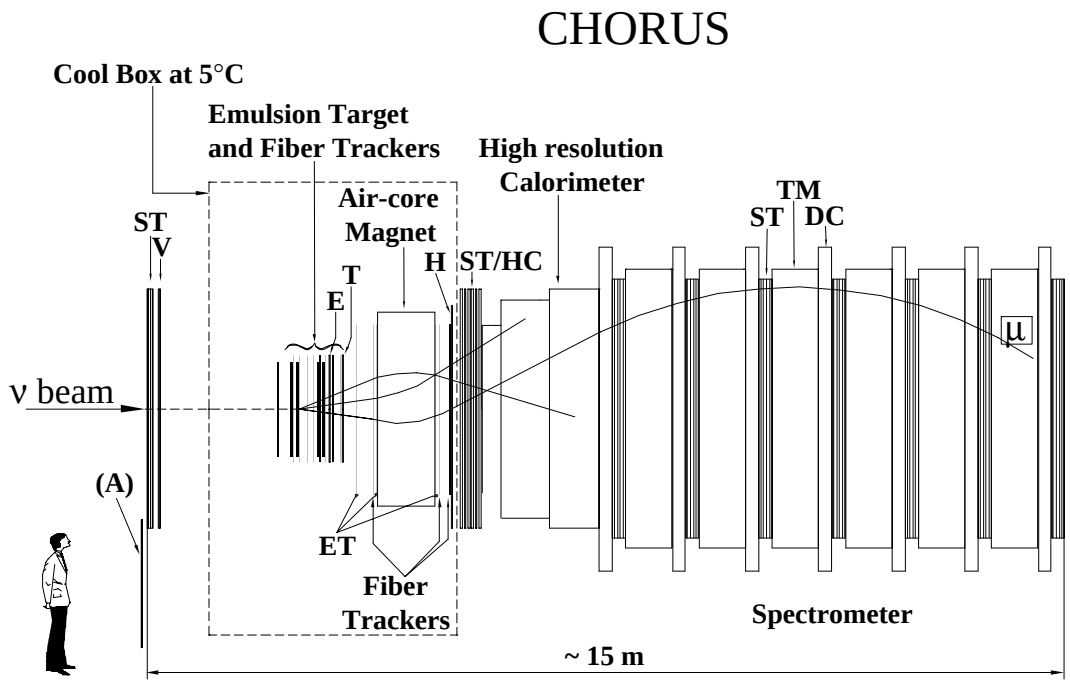

Figure 1: Schematic side view of the CHORUS detector. Streamer tube planes are denoted ST, scintillator trigger planes V,A,E,T and H, emulsion trackers EM, honeycomb chambers HC, drift chambers DC, and toroidal iron magnets TM.

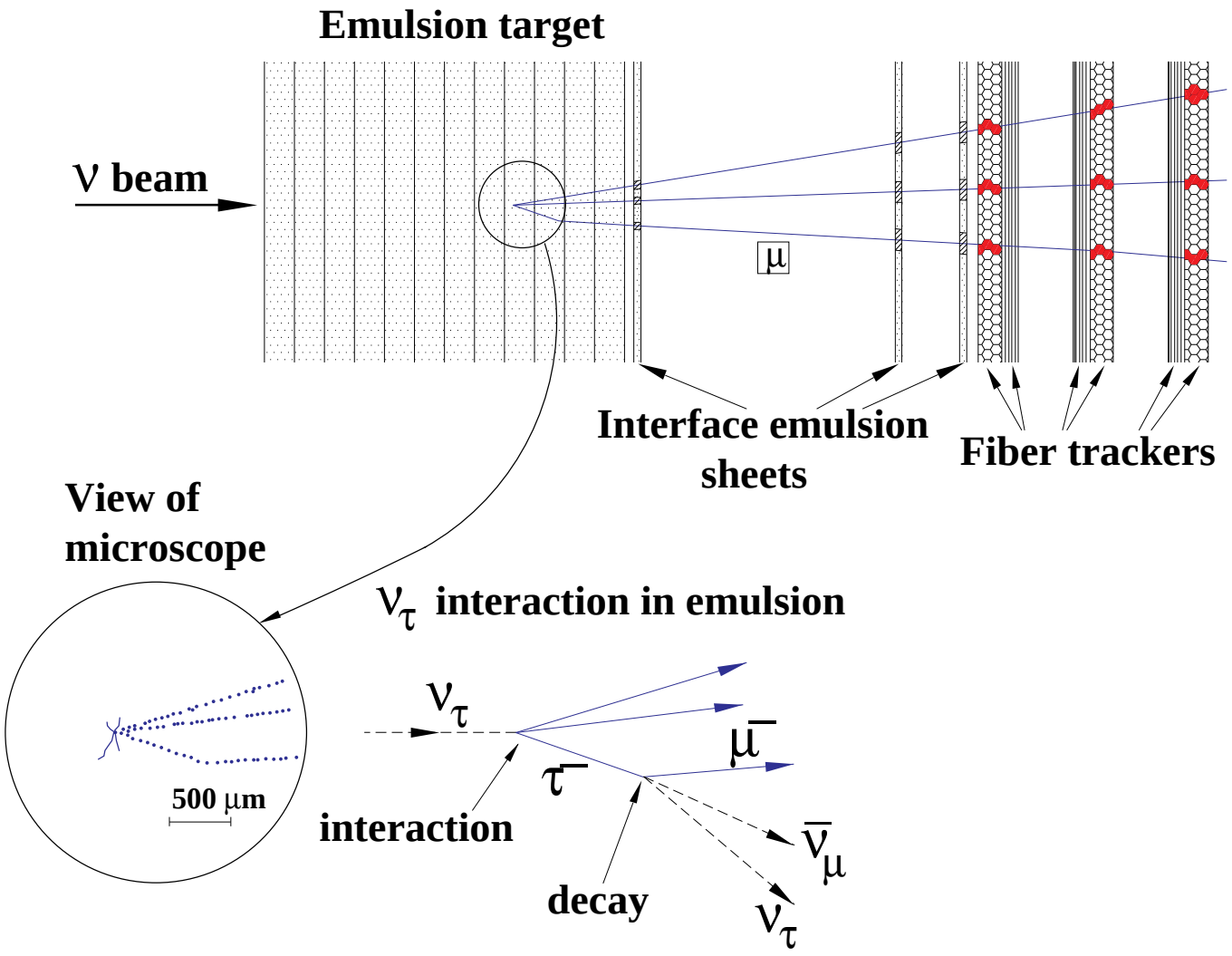

Figure 2: Schematic diagram showing the emulsion target, the interface emulsion sheets (CS and SS) and one target tracker plane. Displayed in the inset is the typical signature of a ν_τ charged-current interaction.

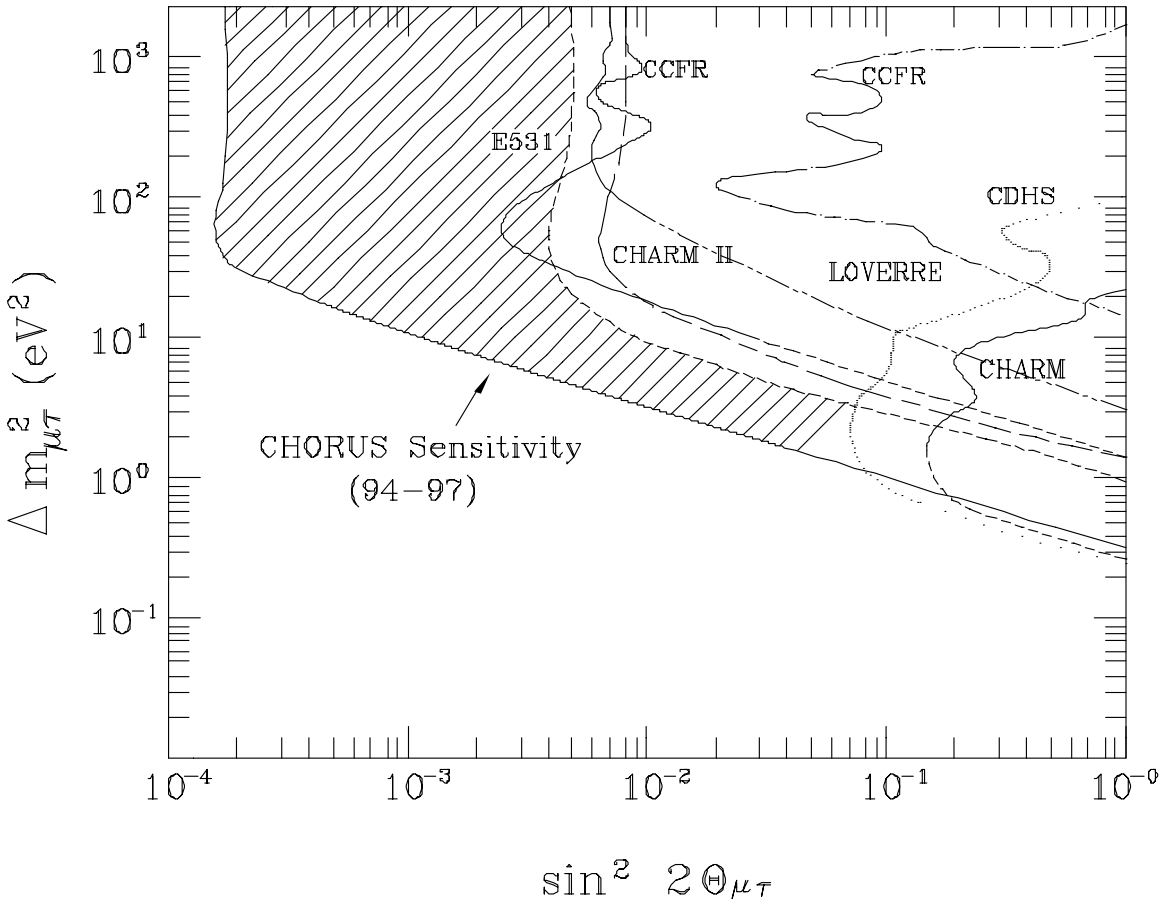

Figure 3: Exclusion plot showing the expected sensitivity of the CHORUS experiment, and the existing limits.

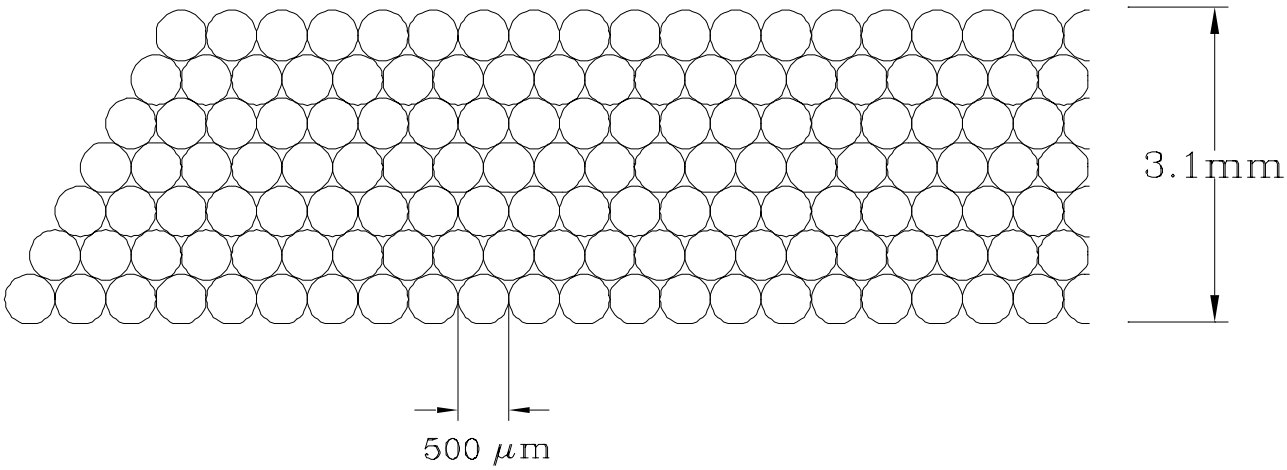

Figure 4: Cross section of a scintillating fiber ribbon, showing its "staggered" geometry.

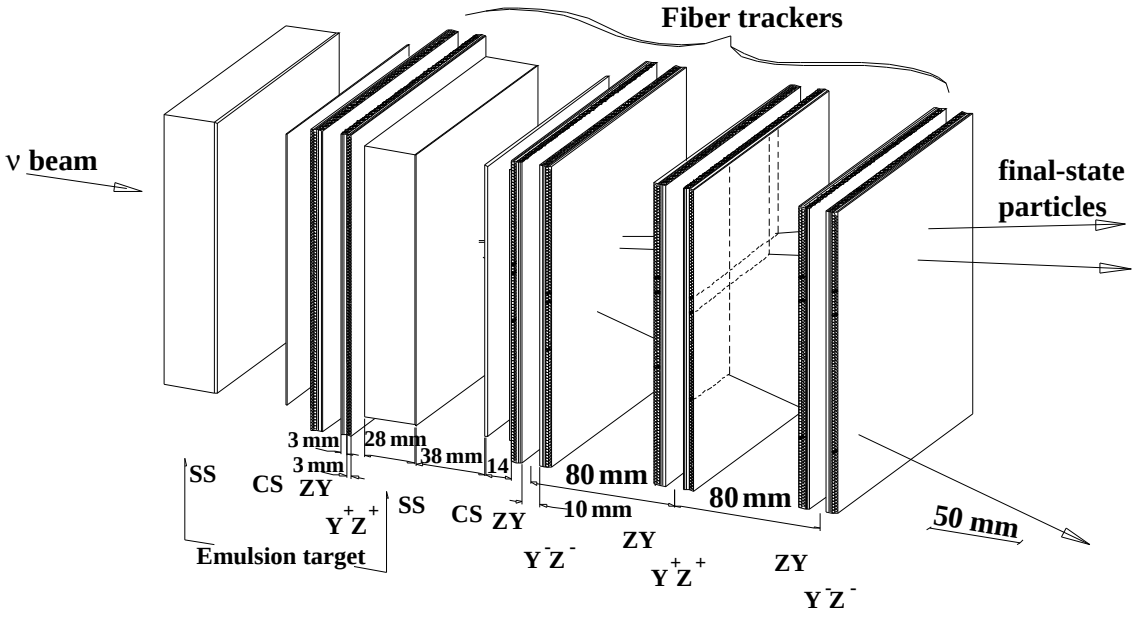

Figure 5: The geometry of one half of the target region, showing the emulsion targets and sheets, with the target trackers. The second half is identical.

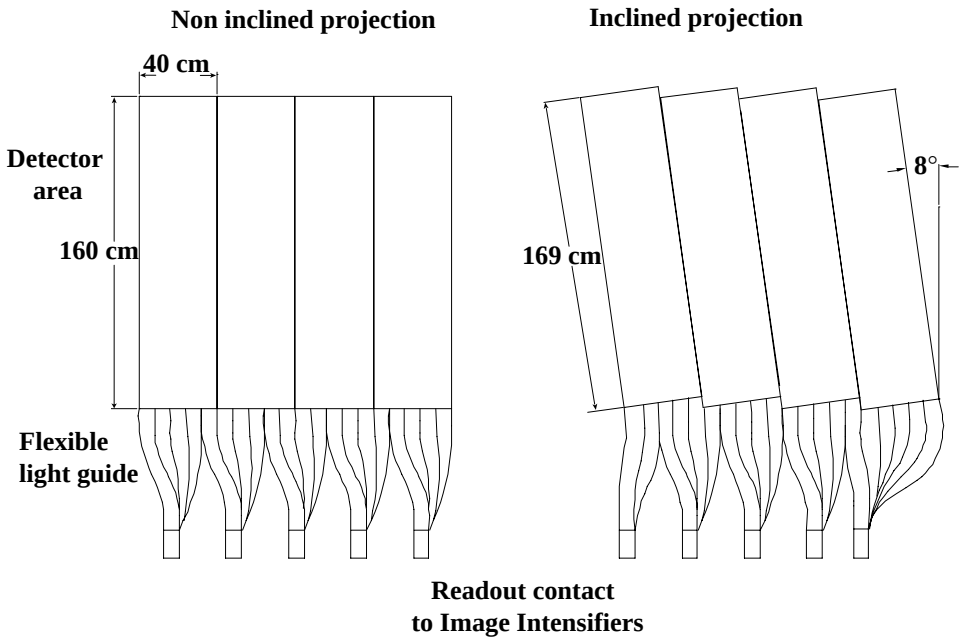

Figure 6: The geometry of a "non-inclined" and an "inclined" projection for the target tracker planes.

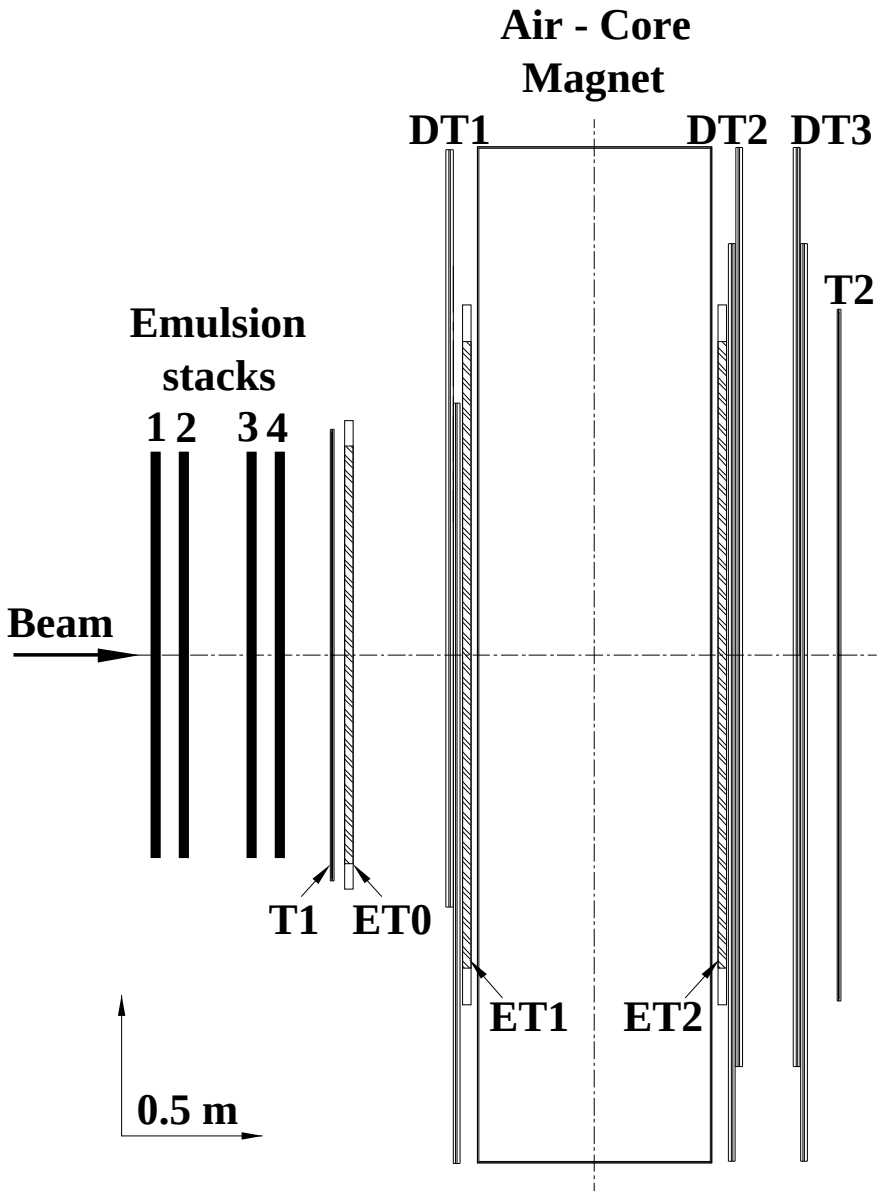

Figure 7: The geometry of the hexagonal toroidal air-core magnet and the magnet trackers (DT1,2,3). The emulsion tracker modules (ET0,1,2), installed in the 1996-97 runs, are also shown.

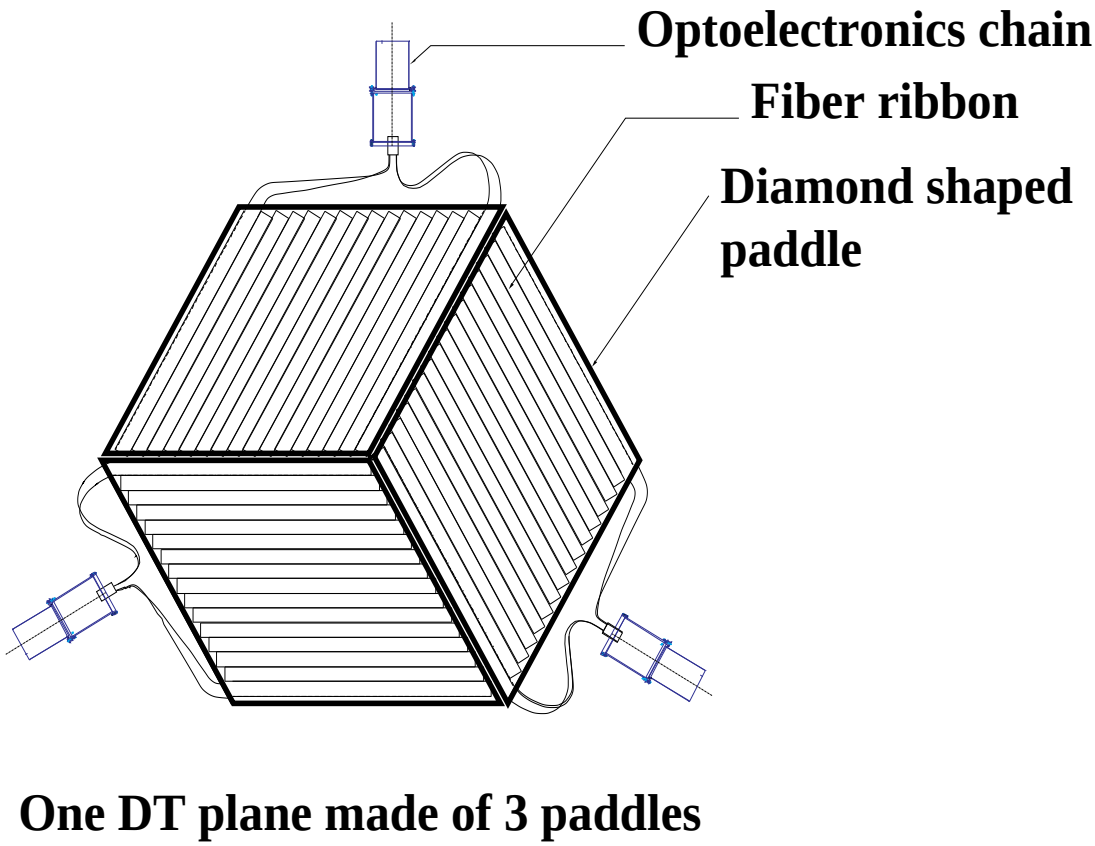

Figure 8: The layout of one plane of the magnet ("diamond") tracker, showing the adjacent three paddles and the fiber arrangement. The second plane in a module reads the complementary coordinates at 120° from the first one.

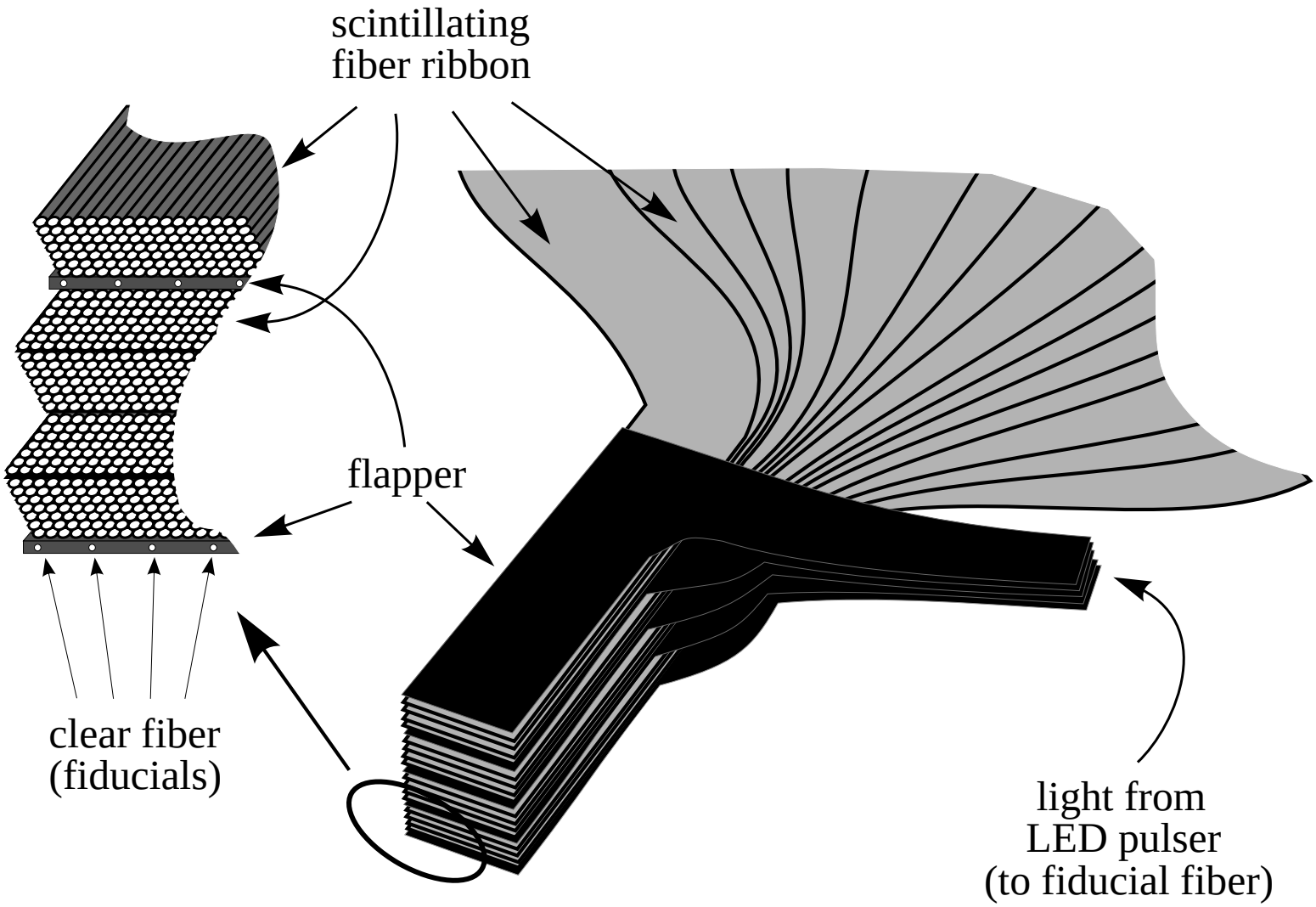

Figure 9: Schematic diagram of the construction of the fiber bundle and calibration fiducial fibers to be coupled to the opto-electronic.

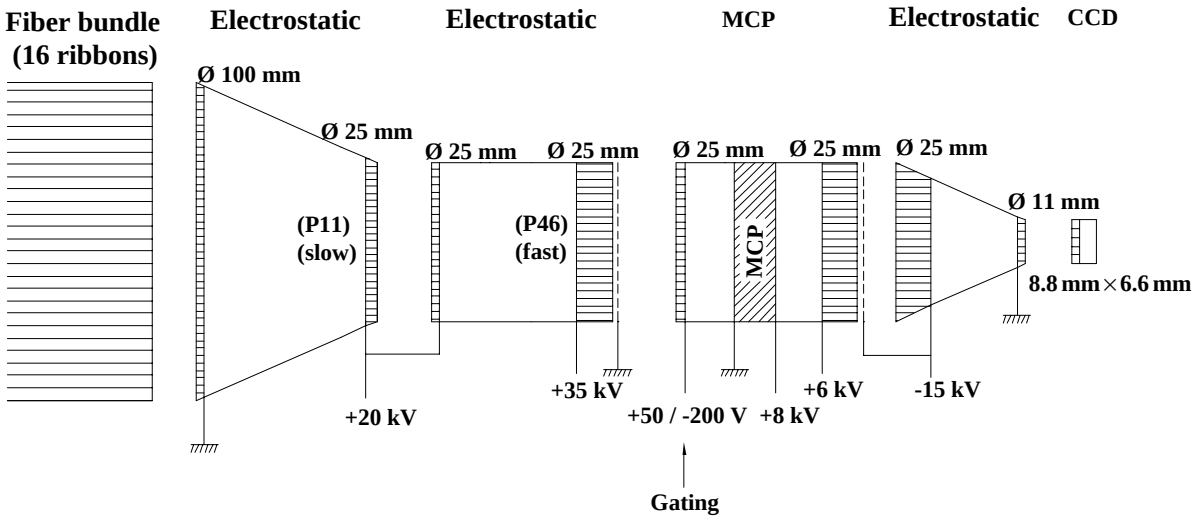

Figure 10: The configuration of the opto-electronic readout system, also showing its voltage layout.

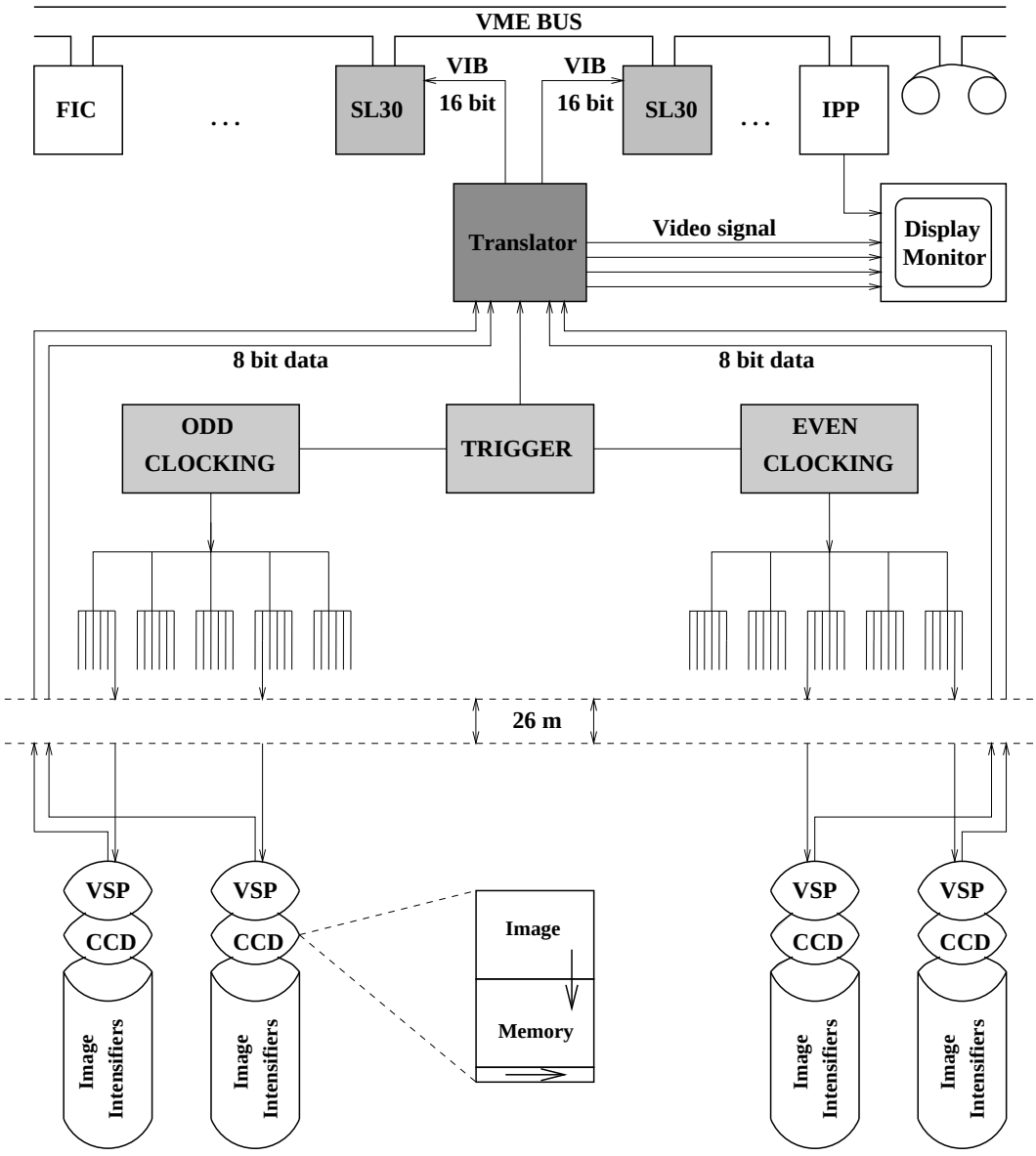

Figure 11: Schematic diagram of the CCD readout and data acquisition system.

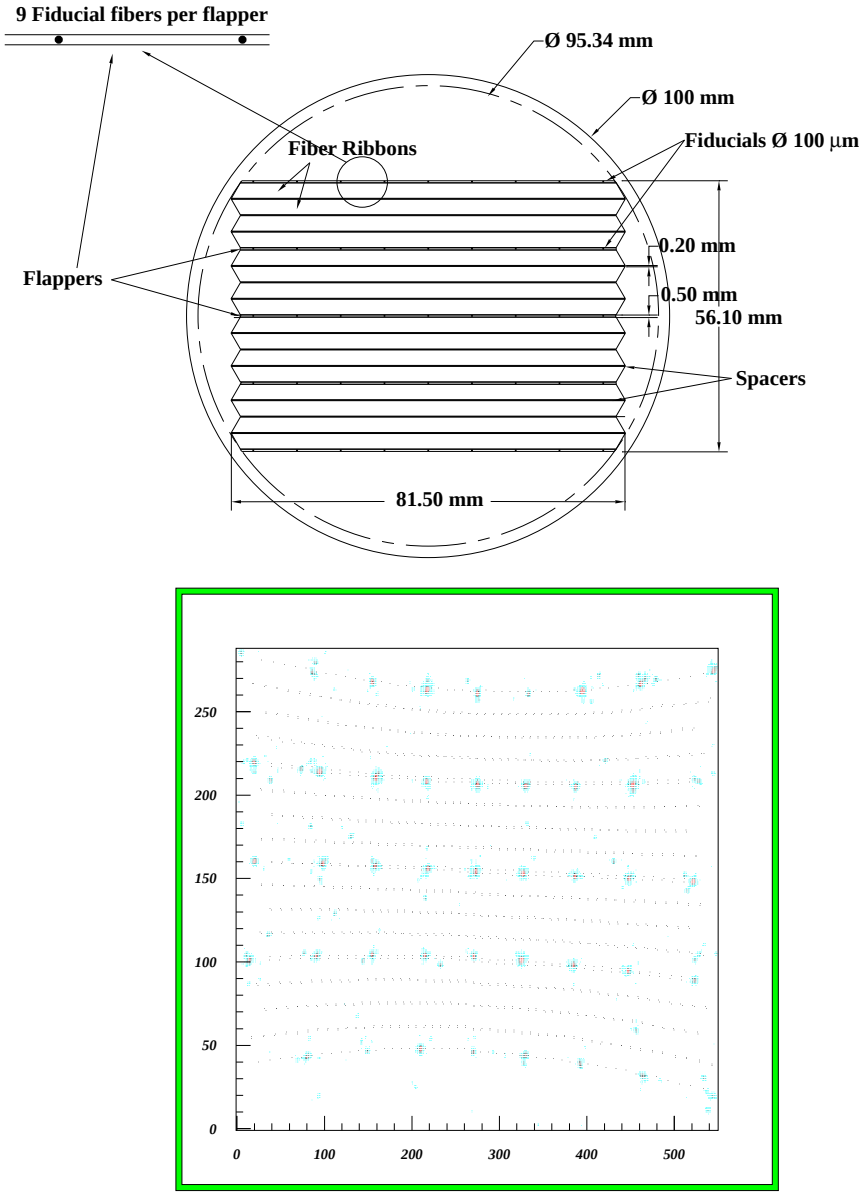

Figure 12: The fiber ribbon bundle as measured in [Top] : the input window of the opto-electronic chains, and [Bottom] : the CCD readout, showing the effects due to electrostatic distortion from the image intensifiers. The units are in CCD pixel number, translating to X=145 μm and Y=209 μm per unit in detector space. Small black dots denote the parametrized ribbon boundary.

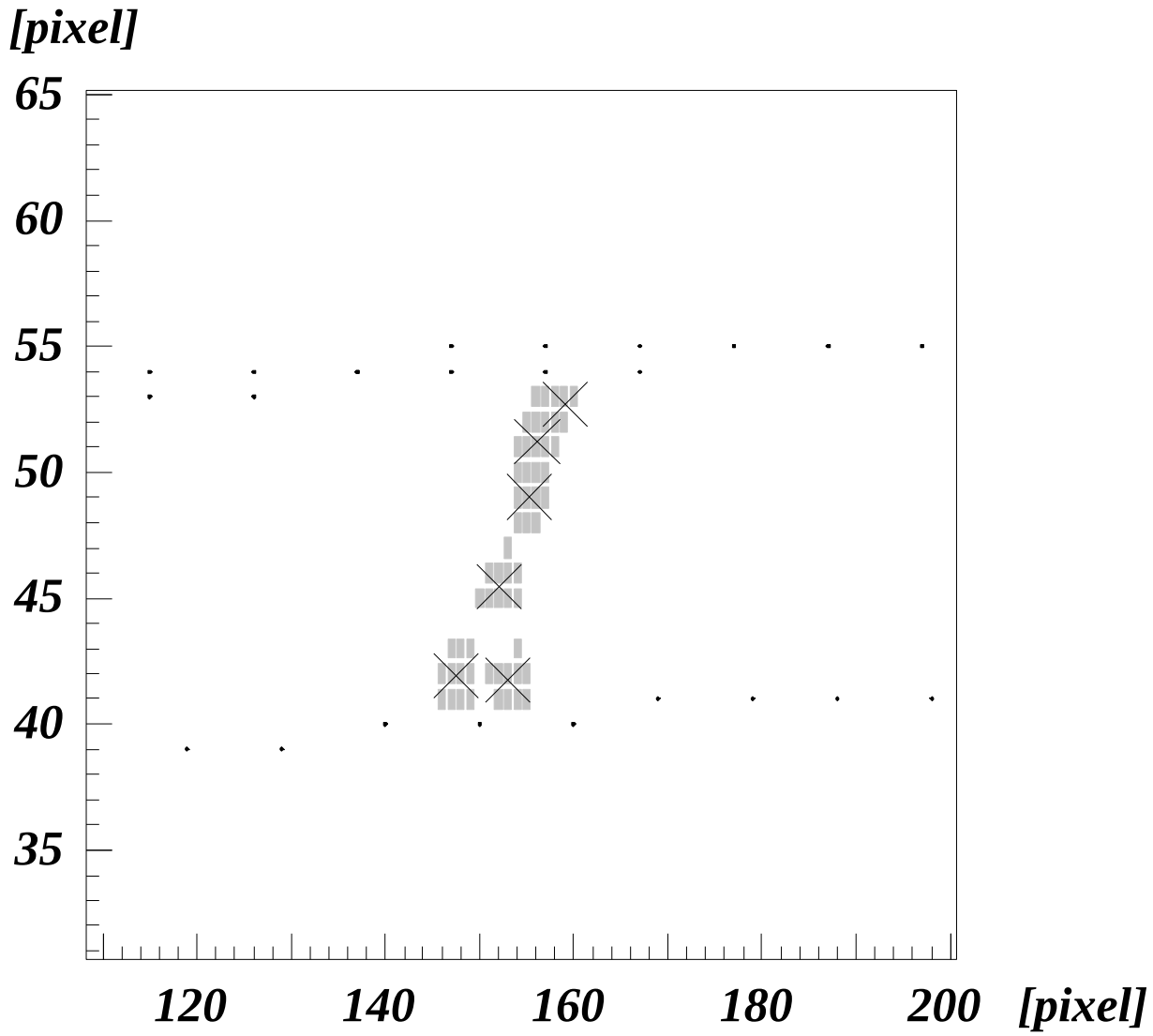

Figure 13: The typical signature of a muon traversing through a fiber ribbon, as recorded by the CCD. Superimposed as crosses are the "hits" as identified by software. Units are in CCD pixel number, as explained in Figure 12 .

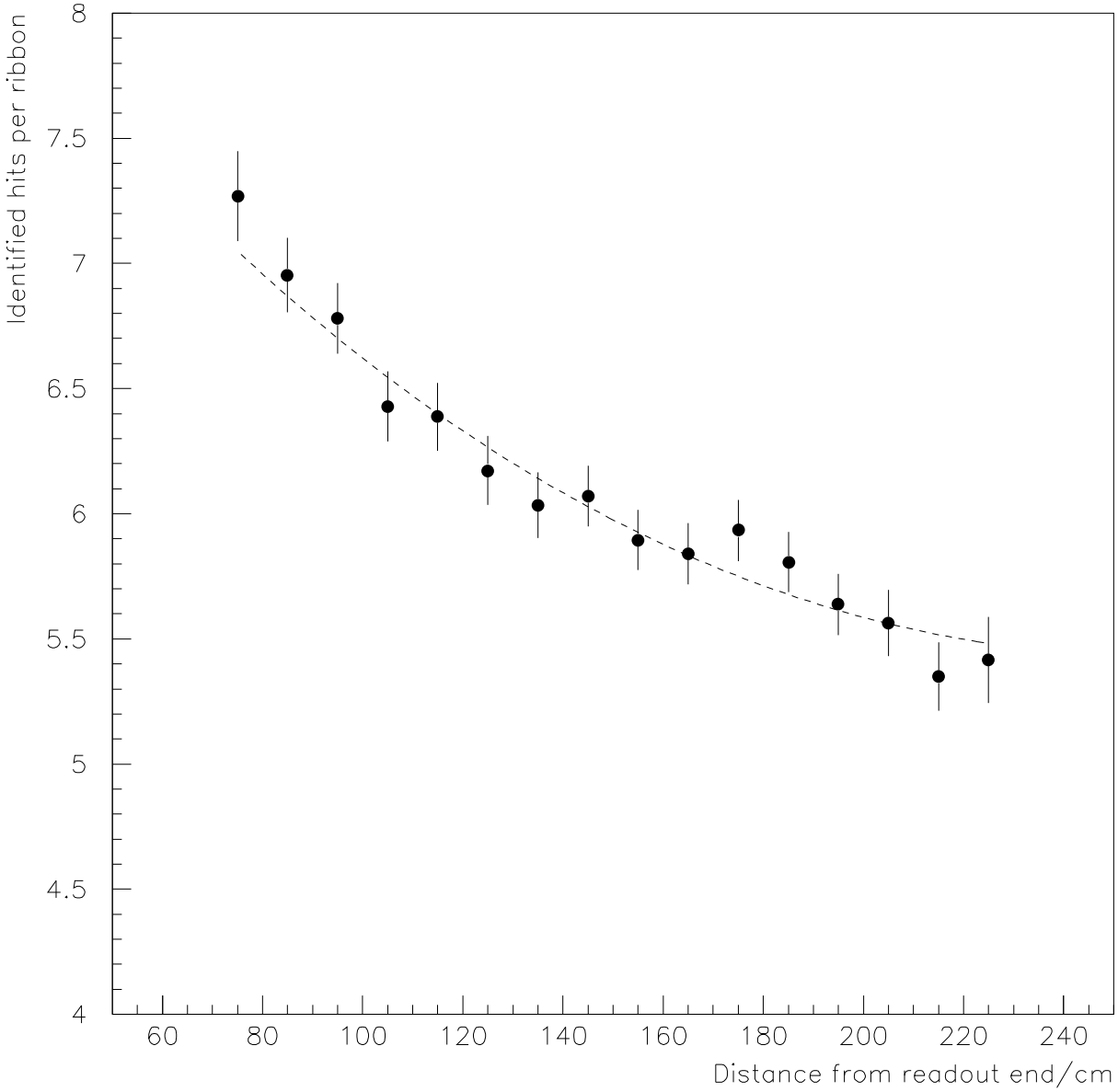

Figure 14: The distribution of ribbon hit density as function of the distance from the readout photocathode. Superimposed is the fitted theoretical curve as explained in Section 3.1.

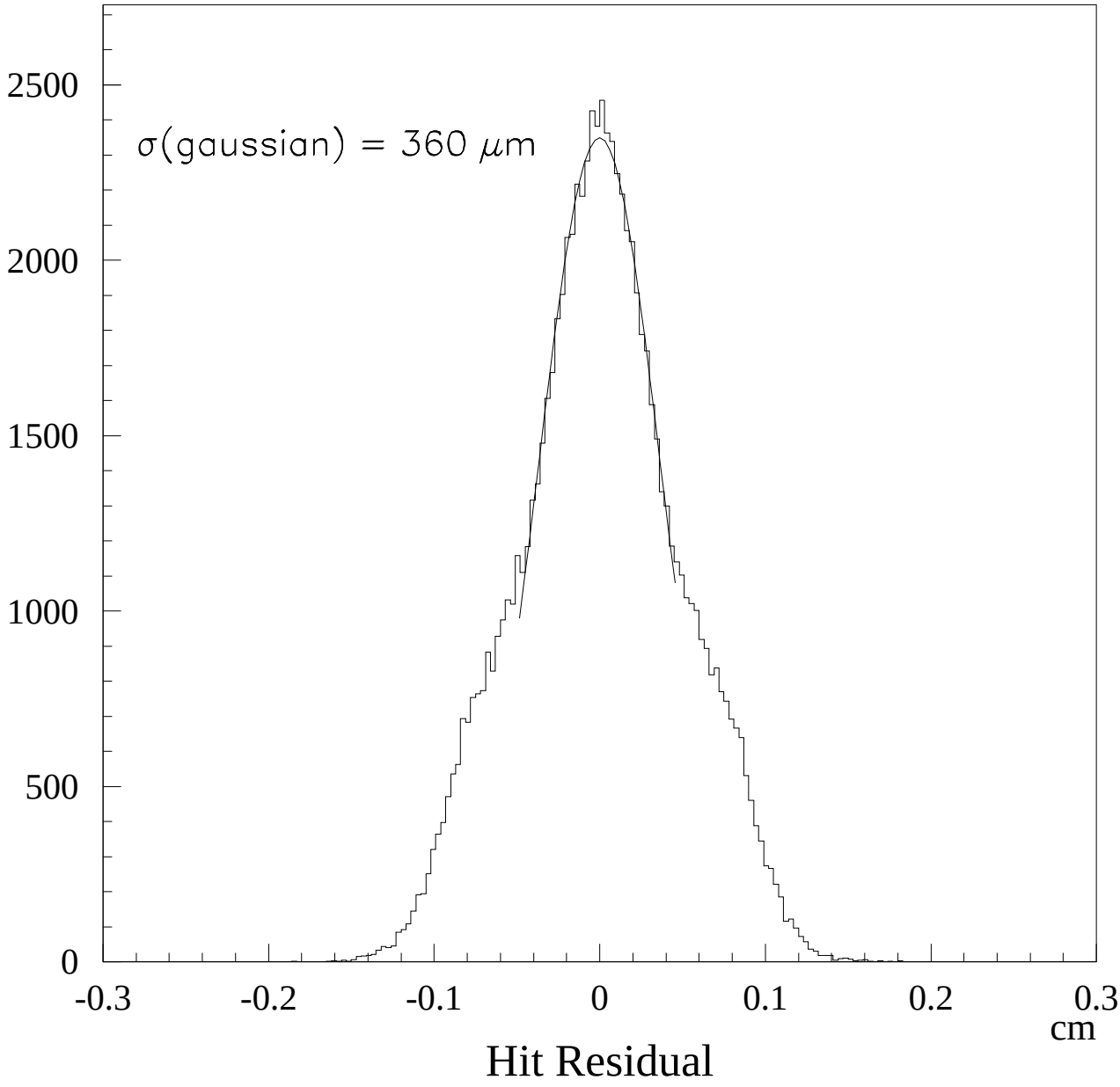

Figure 15: The distribution of the distance between the individual hits left by a charged particle and the best fitted trajectory from raw data. The tails are caused by cross-talk in the entrance fiber optic window of the first image intensifier tube.

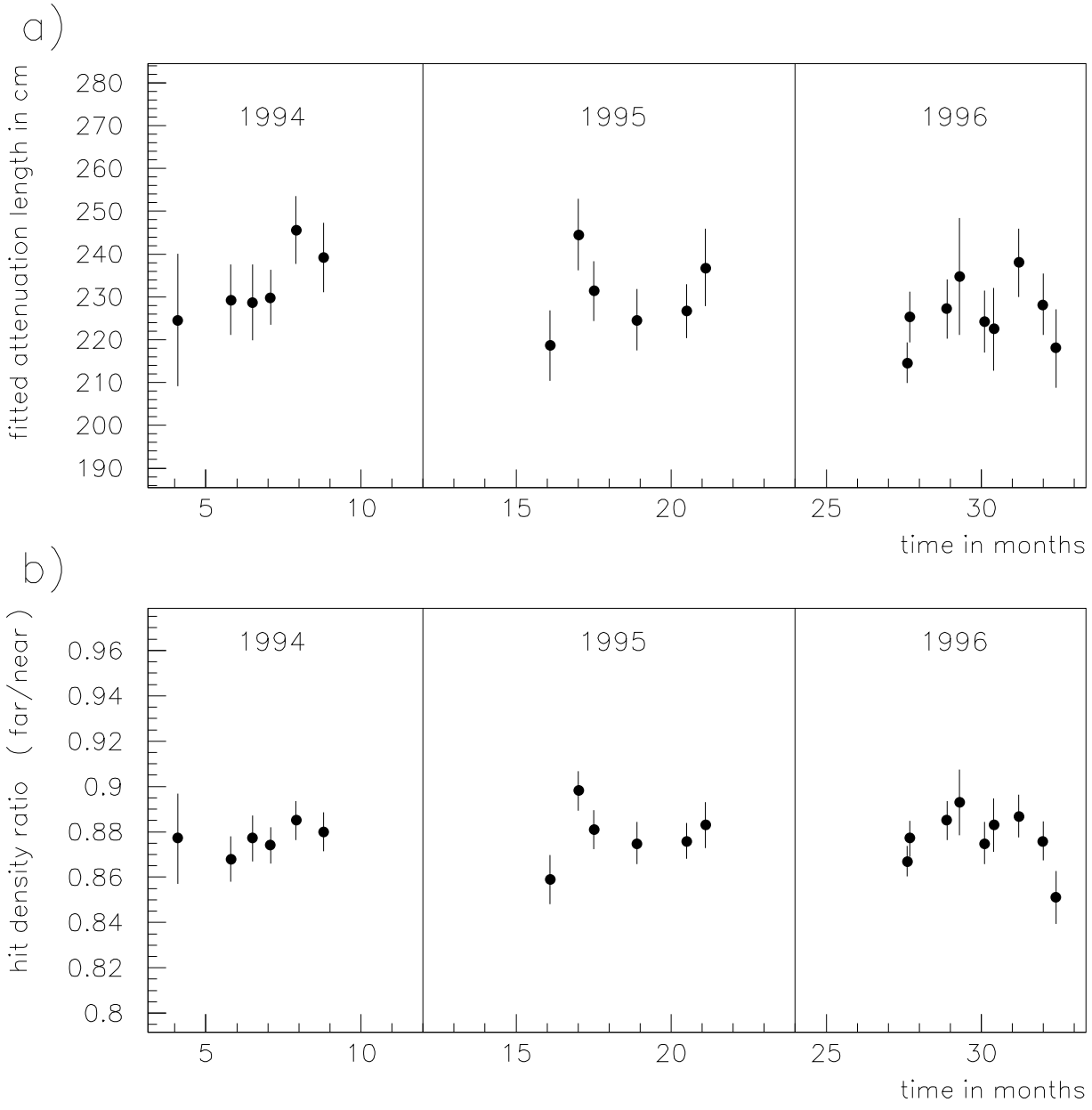

Figure 16: Time evolution of the measured a) attenuation length and b) hit density (far/near) ratio during the course of the experiment.

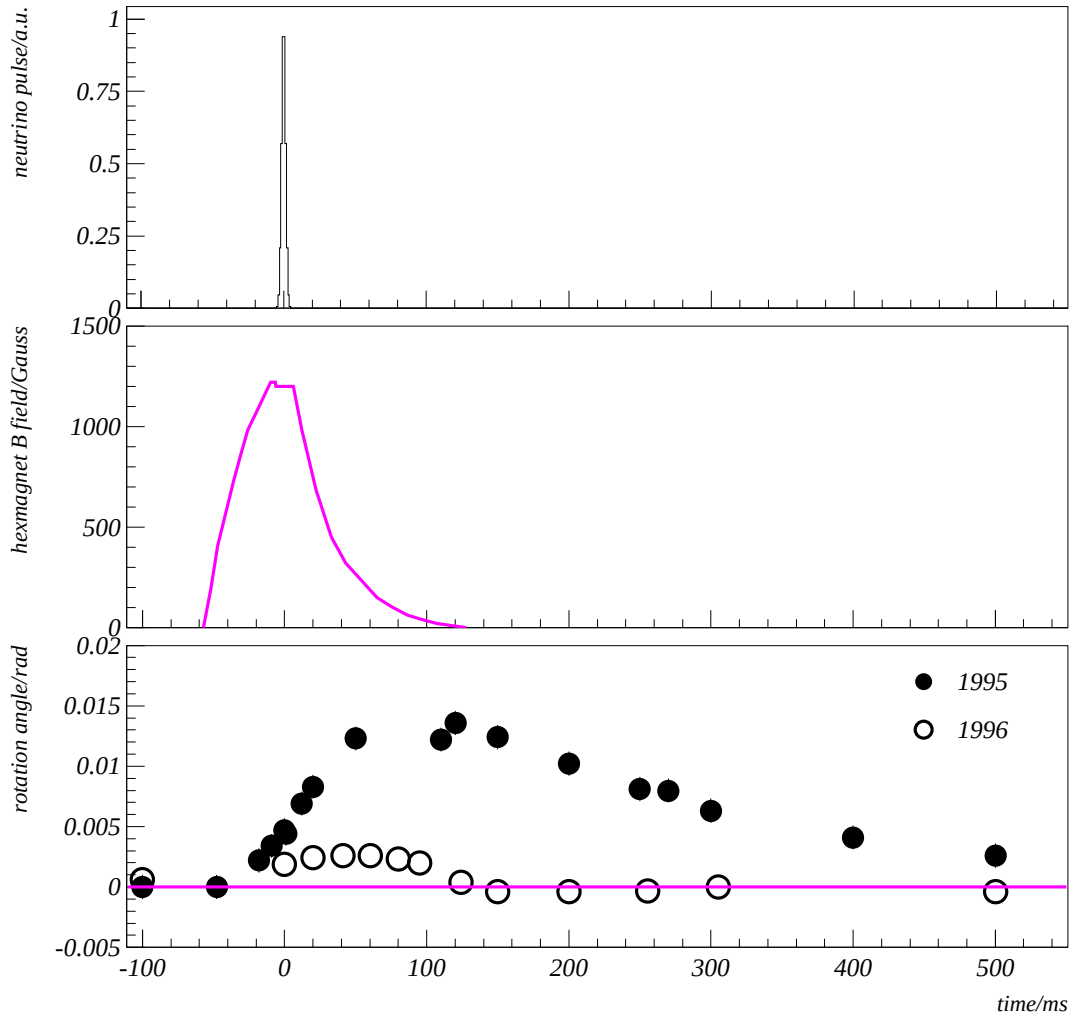

Figure 17: The time structure of [Top]: the neutrino spill (width 4 ms) ; [Middle] : the air-core magnet pulsing; and [Bottom] : the measured rotation angle of a typical opto-electronic chain in the 1995 and 1996 data, before and after correction of the effect by a compensating coil in the air-core magnet, respectively.

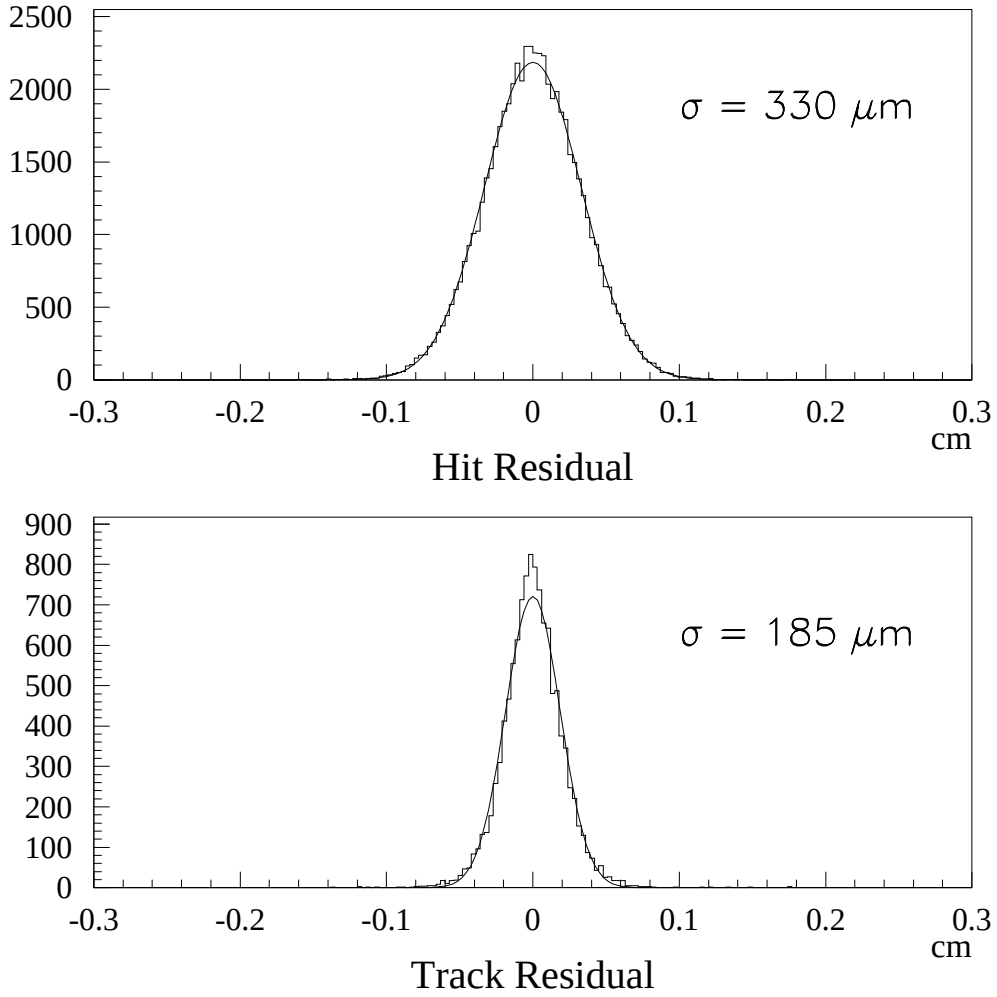

Figure 18: Residual distribution of beam muon data in the target tracker : hit residual distribution, with $\sigma \sim 330\,\mu$m ; and track-element residual distribution, with $\sigma \sim 185\,\mu$m.

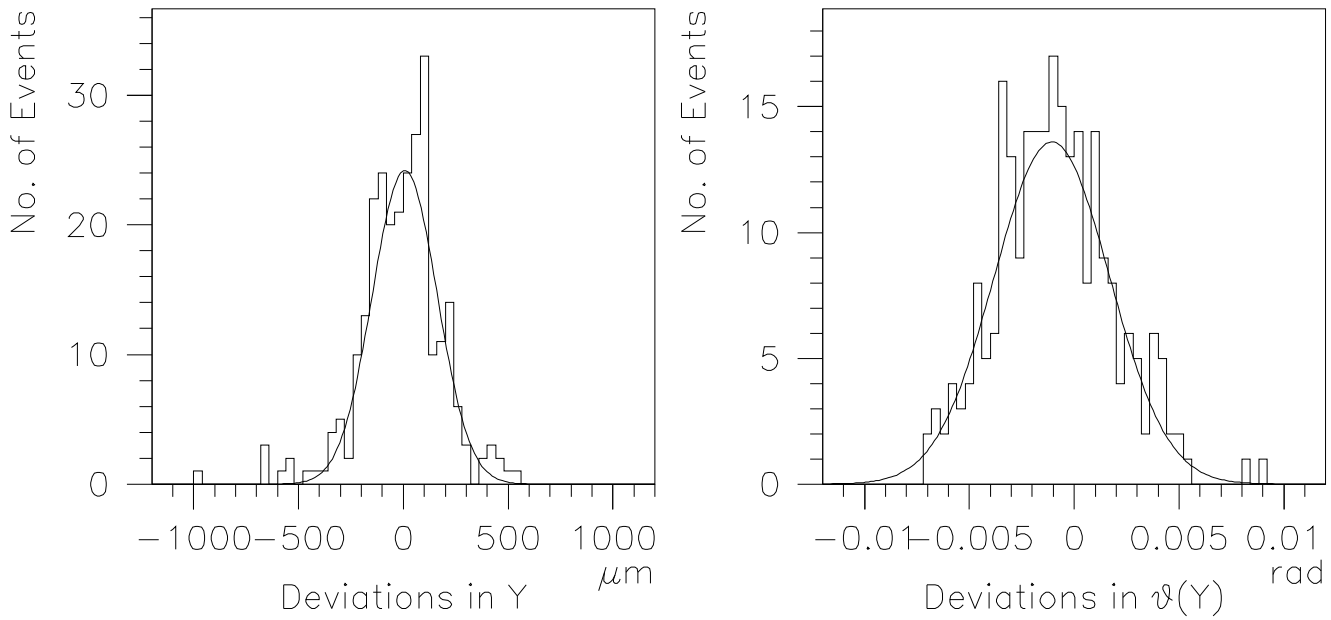

Figure 19: Accuracy in position (Y : $\sigma \sim 150\,\mu$m) and angle (θ(Y) : $\sigma \sim$2.5 mrad), between predicted tracks from target trackers and found tracks at interface emulsion sheets for the beam muon events.

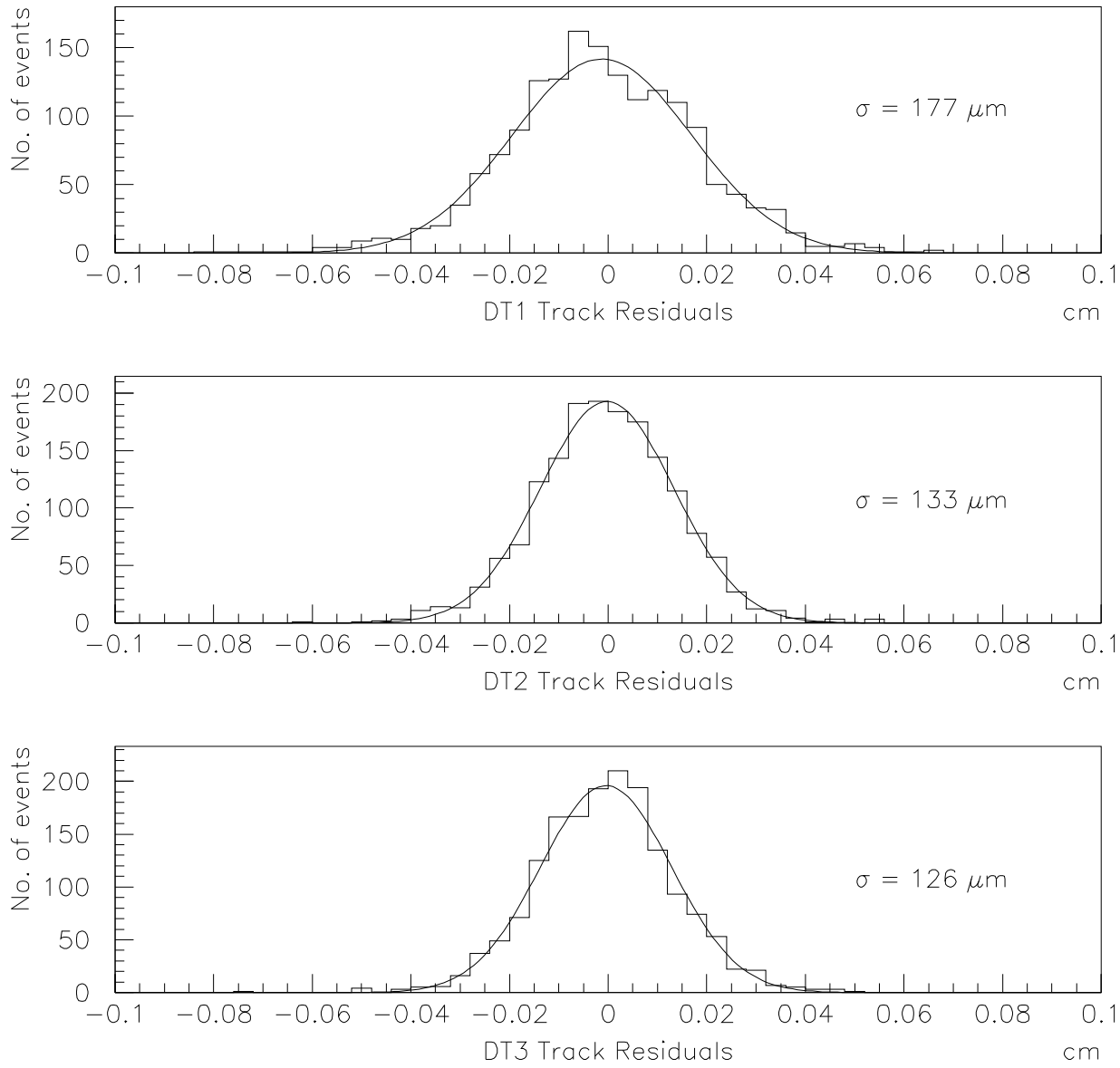

Figure 20: Measured track-element residuals for magnet tracker DT1,2,3, with Gaussian-fit sigmas of 177 μm, 133 μm and 126 μm, respectively.

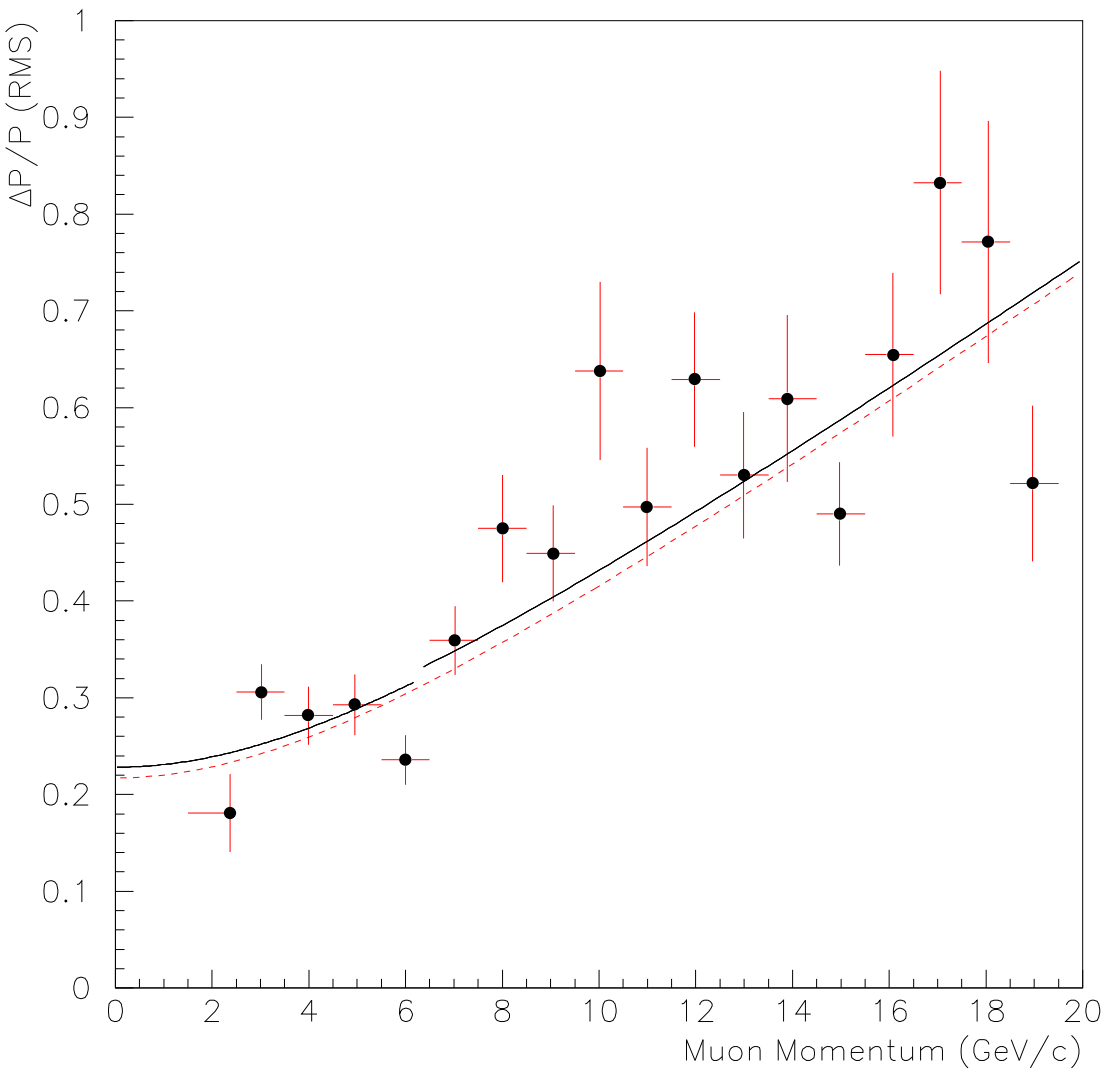

Figure 21: The dashed line shows the momentum resolution for beam muons traversing the air-core magnet, as measured by the magnet tracker. The measured points and the solid line include the effect of the convolution of the resolution of the muon spectrometer.

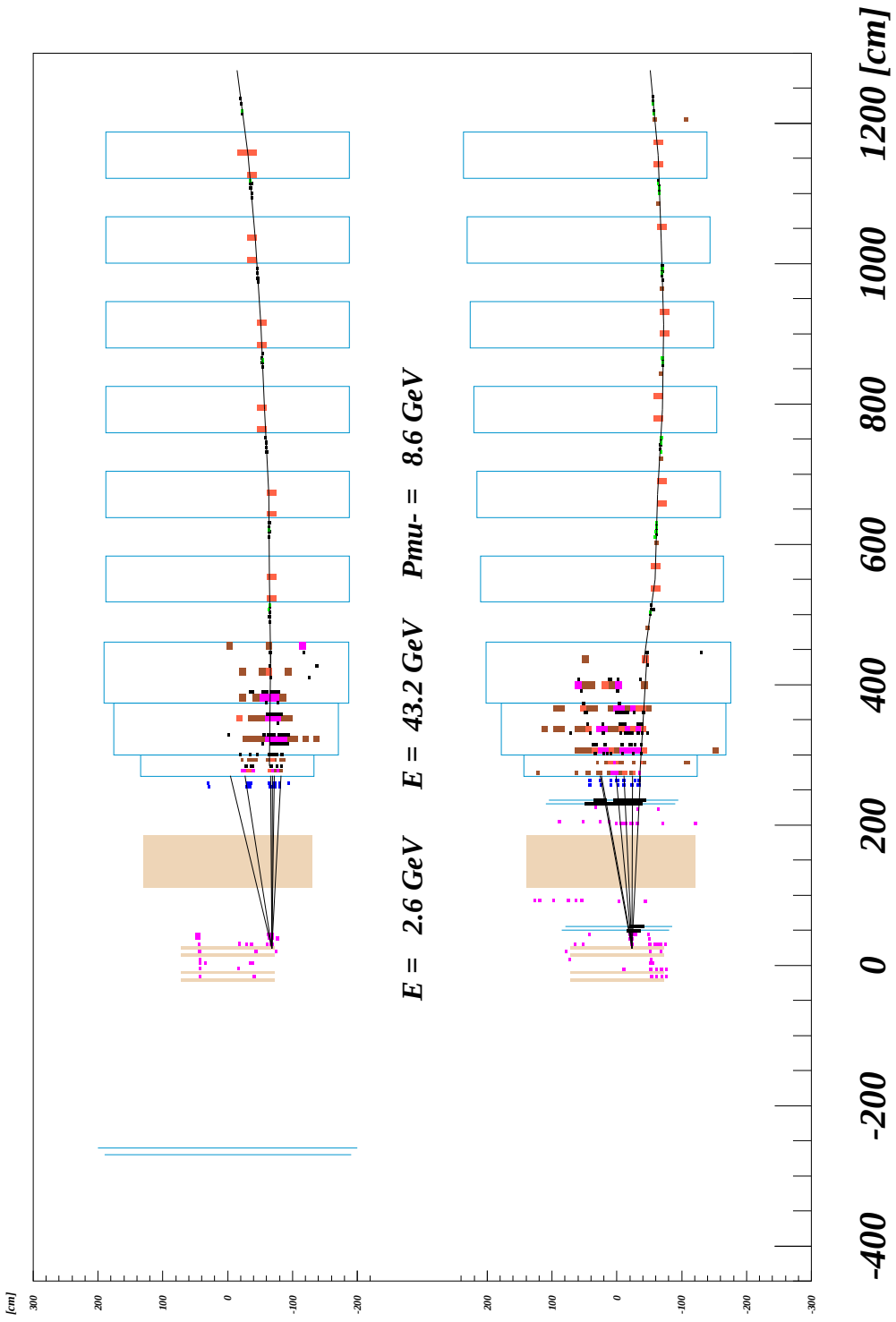

Figure 22: A typical charged-current neutrino-induced event recorded in the CHORUS detector.